Partial Melting of Metapelitic Rocks Beneath the Bushveld Complex, South Africa

TIM E. JOHNSON[1]*, ROGER L. GIBSON[2], MICHAEL BROWN[1], IAN S. BUICK[3] AND IAN CARTWRIGHT[4]

[1]LABORATORY FOR CRUSTAL PETROLOGY, DEPARTMENT OF GEOLOGY, UNIVERSITY OF MARYLAND, COLLEGE PARK, MD 20742, USA

[2]DEPARTMENT OF GEOLOGY, SCHOOL OF GEOSCIENCES, UNIVERSITY OF THE WITWATERSRAND, JOHANNESBURG 2050, SOUTH AFRICA

[3]DEPARTMENT OF EARTH SCIENCES AND VICTORIAN INSTITUTE OF EARTH AND PLANETARY SCIENCES (VIEPS), LA TROBE UNIVERSITY, BUNDOORA, VIC. 3086, AUSTRALIA

[4]SCHOOL OF GEOSCIENCES, MONASH UNIVERSITY, CLAYTON, VIC. 3800, AUSTRALIA

RECEIVED JUNE 27, 2002; ACCEPTED NOVEMBER 6, 2002

Metapelitic rocks in the aureole beneath the Bushveld Complex preserve evidence for both high- and low-a_{H_2O} *anatexis. The aureole is characterized by an inverted thermal structure in which suprasolidus rocks potentially interacted with an* H_2O*-rich volatile phase derived from underlying, dehydrating rocks. At lower grade (*$T < 700°C$*) the rocks contain fibrolite mats and seams that record local redistribution of volatiles. Incongruent reactions consuming biotite produced small quantities (<1 mol %) of liquid and peritectic cordierite that remained trapped within the mesosome. Larger volumes of melt (3–4%), preserved as coarse-grained discordant leucosomes, were produced by congruent melting following a structurally focused influx of* H_2O*. Subhorizontal volatile-phase flow was concentrated within thin (~10 mm) metapsammite horizons that are preserved as stromatic quartz–sillimanite veins. Upward migration occurred along steep fibrolite seams that are subparallel to a variably inclined foliation. Discordant leucosomes are concentrated within antiformal fold closures of quartz–sillimanite veins and along the axial planar schistosity. Closer to the contact (*$T > 725°C$*), volatile-phase-absent, biotite-consuming melting and melt extraction produced coarse-grained garnet–cordierite granofels. At the contact, leucodiatexites devoid of peritectic phases suggest effective segregation of melt from an underlying source. Migmatitic metapelites and their lower-grade stratigraphic equivalents have similar bulk-rock oxygen isotope values, consistent with very limited volatile-phase infiltration and precluding the Bushveld Complex magmas as the source of the volatiles.*

KEY WORDS: *anatexis; Bushveld Complex aureole;* H_2O*; melt segregation; migmatite*

INTRODUCTION

Recent studies have advanced our understanding of the generation and segregation of anatectic melt from grain to outcrop scale (Brown *et al.*, 1995; Hartel & Pattison, 1996; Johnson *et al.*, 2001*a*; Sawyer, 2001; Marchildon & Brown, 2002) and have underlined the important role played by deformation in melt migration and ascent (e.g. D'Lemos *et al.*, 1992; Brown, 1994; Sawyer, 1994; Brown & Solar, 1999). Additionally, thermodynamic datasets have been extended to allow modelling of metapelitic phase relations involving silicate liquids in increasingly complex systems that more closely approximate natural rocks (Holland & Powell, 1998, 2001; Tinkham *et al.*, 2001; White *et al.*, 2001, 2002). Studies in regional metamorphic terrains are commonly complicated by polyphase deformation and by the protracted time scale for cooling that may allow retrogression of migmatitic rocks. In contact aureoles, where strain may be lower and the time scale for cooling faster, a more thorough investigation of melting relationships is commonly possible (e.g. Pattison & Harte, 1988; Droop *et al.*, 2003).

This study examines metapelitic migmatites in the aureole of the eastern Bushveld Complex, South Africa

*Corresponding author. Telephone: 301-405-8181. Fax: 301-314-9661. E-mail: timj@geol.umd.edu

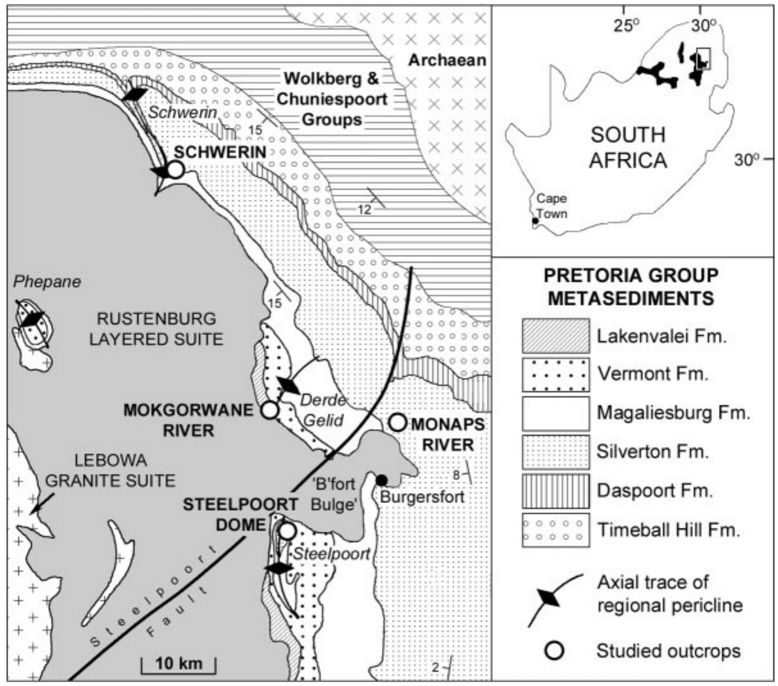

Fig. 1. Location map showing part of the eastern Bushveld Complex and underlying Transvaal Supergroup rocks, and the localities of the lower-grade (Schwerin and Monaps River) and higher-grade (Steelpoort and Derde Gelid) outcrops. Regional periclinal folds are shown in italics.

(Fig. 1). The aureole is unusual both in its scale and in the fact that it is developed in the floor rocks underlying the intrusion; the thermal peak diminished and was reached at progressively later times with increasing depth below the contact, i.e. the thermal gradient was inverted relative to the normal situation during regional metamorphism. Subsolidus rocks that were undergoing prograde metamorphism involving progressive dehydration are likely to have supplied overlying suprasolidus rocks with a source of H_2O that potentially influenced melting behaviour.

We combine field and petrographic observations with quantitative equilibrium mineral–melt calculations in the model NCKFMASH (Na_2O–CaO–K_2O–FeO–MgO–Al_2O_3–SiO_2–H_2O) system to provide constraints on the prograde reaction sequence responsible for leucosome formation. We assess the origin and influence of H_2O-rich volatile-phase influx on melt generation and segregation.

GEOLOGICAL SETTING

The Bushveld Complex is a sill-like body comprising the 6–8 km thick mafic–ultramafic Rustenburg Layered Suite (RLS) and up to 2 km of overlying Lebowa Granite Suite that was emplaced at 2·06 Ga (Walraven *et al.*, 1990; Buick *et al.*, 2001; Fig. 1). The Complex intruded sedimentary rocks of the 2·55–2·06 Ga Transvaal Supergroup and penecontemporaneous volcanics of the Rooiberg Group (Walraven, 1997; Nelson *et al.*, 1999). The Bushveld Complex and the Transvaal Supergroup strata together exhibit a general basinal structure. Although dips approach 60–80° along the northern margin of the Complex, they are more typically of the order of 10–20°. In the eastern Bushveld Complex, the strata are locally affected by a series of broadly north–south-trending anticlinal periclines, with wavelengths of several kilometres, that have disturbed the footwall contact (e.g. De Waal, 1970; Sharpe & Chadwick, 1982; Hartzer, 1995; Bumby *et al.*, 1998; Fig. 1). Button (1978) and Uken & Watkeys (1997) proposed that the periclines formed by magma loading of ductile floor rocks and upwards amplification of the folds into the base of the RLS.

An extensive but poorly exposed contact aureole is developed at the base of the RLS, principally within rocks of the Pretoria Group (uppermost Transvaal Supergroup) that include, from the stratigraphical base upwards, the Timeball Hill, Daspoort, Silverton, Magaliesberg, Vermont and Lakenvalei Formations (Fig. 1). In the NE, where the RLS is thickest, the contact aureole extends to a distance of at least 25 km from the RLS contact, corresponding to an orthogonal thickness of ~4 km.

Waters & Lovegrove (2002) noted a systematic upward increase in the bulk X_{Mg} [molar Mg/(Mg + Fe)] of Pretoria Group metapelitic rocks that is reflected in a change from andalusite- to cordierite-dominated assemblages as the RLS contact is approached. Multi-equilibria calculations by those workers on a high-grade (sillimanite-bearing) metapelitic rock provide a robust pressure estimate of 3·0 ± 0·5 kbar that is consistent with overburden calculations and the observation that prograde muscovite was consumed in quartz-present rocks before the onset of melting (e.g. Holland & Powell, 2001).

Willemse & Viljoen (1970), Nell (1985) and Engelbrecht (1990) described high- and ultrahigh-T assemblages in residual metapelitic xenoliths and migmatitic rocks in contact with the RLS. Sharpe & Chadwick (1982) and Uken & Watkeys (1997) noted the structural control on leucosome accumulation within the regional periclinal folds. Engelbrecht (1990) reported $T \sim 760°C$ from metapelitic rocks close to the contact based on garnet–biotite and garnet–cordierite Fe–Mg exchange thermometry. Similar temperatures ($T > 750°C$) are inferred based on the presence of garnet- and orthopyroxene-bearing migmatites using the partial melting equilibria calculated by White *et al.* (2001). Peak pressures of ~3 kbar and the abundance of garnet, cordierite and orthopyroxene imply that the migmatites developed via incongruent volatile-phase-absent melting consuming biotite. Because of the low solubility of Fe and Mg in granitic melt, such reactions are characterized by the prograde formation of ferromagnesian peritectic solid products.

This study concentrates on the high-grade parts of the eastern aureole and, in particular, anatectic migmatites developed within rocks of the Silverton, Vermont and Lakenvalei Formations (Fig. 1). Evidence of melting, in the form of a migmatite front, has been found up to distances of 2 km from the lower contact of the RLS, corresponding to a maximum orthogonal distance of 400–700 m from the intrusion. The pattern is complicated by numerous pre- to syn-RLS sills (e.g. Sharpe & Hulbert, 1985) and locally by the transgressive 'Burgersfort Bulge' (Fig. 1).

Migmatites generally comprise macroscopic portions that are lighter, intermediate and darker in colour. We refer to these as leucosome, mesosome and melanosome, respectively, with no genetic connotation. Additional terminology follows Mehnert (1968) and Brown (1973).

FIELD RELATIONSHIPS

We studied four localities that illustrate different suprasolidus metamorphic grades in the aureole. In the following discussion, the migmatites are subdivided into: (1) lower-grade fibrolitic sillimanite-bearing metatexites exposed in the Monaps River and in the core of the Schwerin fold (Fig. 1, Silverton Formation); (2) higher-grade migmatites, comprising sillimanite-absent granofels and diatexite exposed on the NE margin of the Steelpoort dome (Fig. 1, Vermont Formation) and along the Mokgorwane River on the western margin of the Derde Gelid antiform (Fig. 1, Lakenvalei Formation).

Lower-grade migmatites

Migmatites at the Monaps River and Schwerin localities (Fig. 1) exhibit similar relationships, although outcrops at the latter appear more deformed. The rocks commonly show gentle to open folds with wavelengths of up to a few metres although strain is locally more intense. A weak to moderately developed, variably inclined foliation is evident (Fig. 2a).

The Monaps River locality is characterized by a shallowly dipping sequence with low bulk strains typical of much of the aureole. The exposures are 600–1000 m from the nearest outcrops of the RLS, around 300–350 m stratigraphically beneath the contact. The Schwerin outcrops are a similar distance from the contact, but close to the axial trace of the Schwerin periclinal fold (Fig. 1). At both localities the sequence comprises thinly to moderately bedded metapelite; metasemi-pelitic and calc-silicate rocks are subordinate. Sedimentary structures (graded, flaser and rare cross-bedding) indicate a right-way-up sequence. Thin bedding-concordant (stromatic) quartz–sillimanite veins, discordant podiform leucosome segregations and anastomosing seams of fibrolite are conspicuous (Fig. 2a and b).

The migmatites are volumetrically dominated by mesosome, which contains biotite, quartz, fibrolitic sillimanite, plagioclase, muscovite ± cordierite, tourmaline and opaque phases. Many horizons contain abundant porphyroblasts of andalusite (up to 3 mm long), reflecting iron-richer bulk compositions; poikiloblasts of cordierite (up to 5 mm) occur without andalusite in more magnesian metapelitic rocks. Small (~1 mm) leucocratic quartzofeldspathic and/or muscovite-rich patches are abundant within mesosome (Fig. 2c).

Thin (<30 mm, usually ~10 mm wide) stromatic quartz–sillimanite veins (Fig. 2a, c, d and e) are fine grained, laterally continuous and have an assemblage dominated by quartz, fibrolite and fibrolitized biotite. They are commonly flanked by biotite-rich melanosomes a few millimetres in thickness (e.g. Fig. 2c). The quartz–sillimanite veins display small-scale folding in the form of upright, open to tight, locally ptygmatic folds with wavelengths and amplitudes of

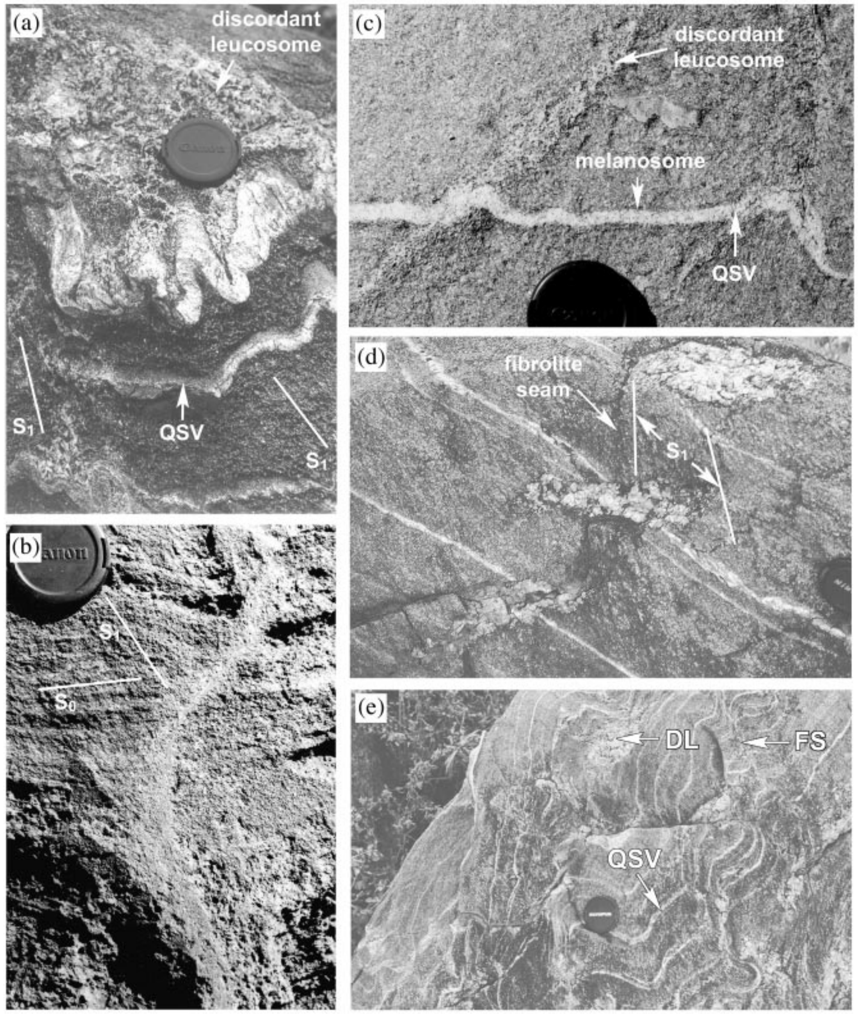

Fig. 2. Field relations of the lower-grade migmatites. (a) Upright, open to tightly folded stromatic quartz–sillimanite veins (QSV) and coarse-grained, discordant leucosome. QSV are foliated and have a biotite-rich melanosome. Discordant leucosome is concentrated around the anticlinal crests of folded QSV. The moderate- to steeply dipping foliation (S_1) in the andalusite-rich mesosome (lower right) becomes subvertical (lower left) where it is associated with leucosome. (b) Irregular sinuous fibrolite seam. Offshoots from the main seam splay into parallelism with bedding (S_0). These bodies are common at lower grades and are interpreted to record the passage of H_2O-rich volatiles through the system. (c) Subhorizontal QSV with well-defined melanosome exhibits gentle, upright folds. A discordant leucosome is aligned parallel to the weak foliation. Numerous millimetric leucocratic patches are just visible within the mesosome. (d) Cross-cutting pegmatitic discordant leucosomes within a tension gash array. The leucosome pods are connected by thin fibrolite seams. The seams are subparallel to the steep foliation, which becomes more moderately inclined away from these areas. (e) Diktyonitic structure comprising folded QSV, steeply inclined fibrolite seams (FS) and podiform discordant leucosome (DL). (a)–(c) from the Monaps locality, (d) and (e) from Schwerin. Diameter of lens cap is 55 mm.

<10 cm; they are locally foliated parallel to the foliation within the mesosome (Fig. 2a). The foliation generally dips more steeply than bedding although the orientation of the foliation is highly variable across the outcrops. Away from small-scale folds, the foliation is shallow and at a low angle to bedding. However, in the vicinity of the ptygmatic folds the foliation is steep and most intensely developed (Fig. 2a).

Higher-strain foliation domains are commonly associated with discordant leucosome (Fig. 2a) and/or subparallel to anastomosing networks of thin (< 5 mm) seams of fibrolite. The seams splay at their margins and terminations into parallelism with bedding, which may be deflected against the seams (Fig. 2b). The discordant leucosomes form pods and veins (Fig. 2a, c, d and e) that comprise a few percent (less than or much less than 5 vol. %) of the outcrop. They are usually < 50 cm in length, coarser grained (1–3 mm, locally pegmatitic) than the mesosome, have diffuse or sharp contacts and lack melanosome. Leucosomes are composed of quartz, plagioclase, muscovite, biotite, tourmaline and fibrolite ± cordierite.

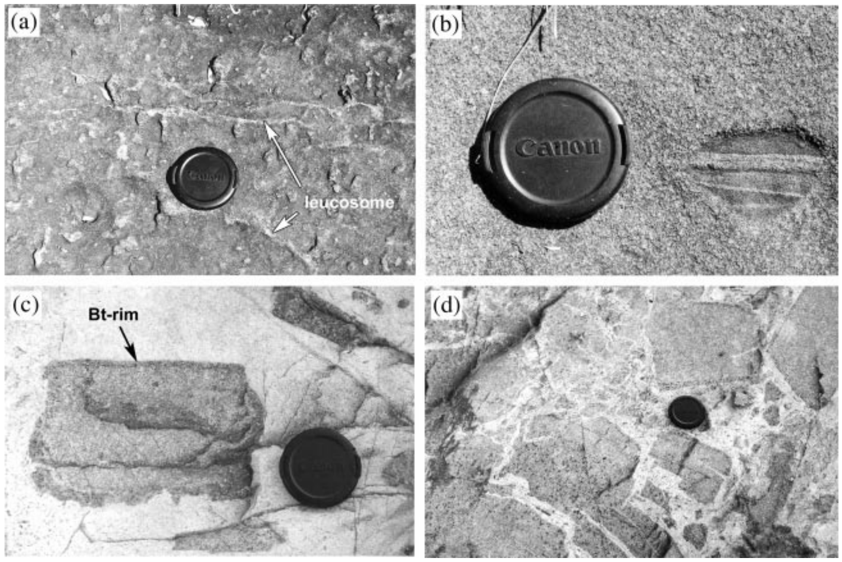

Fig. 3. Field relations of the higher-grade migmatites. (a) Coarse-grained garnet–cordierite granofels on the margin of the Steelpoort dome. Euhedral garnets are ~10 mm in diameter. Irregular discontinuous leucosome veins containing small garnets are conspicuous; overall leucosome fractions are <5 vol. %. (b) Leucosome-rich inhomogeneous schollen diatexite bordering (a). These rocks have a broadly granitic assemblage and microstructure, are garnet free and are richer in hydrous phases, particularly muscovite. Leucosome is continuous through the biotite-rich schollen. (c) Exposures in the Mokgorwane River ~20 m from the contact show norite xenoliths within a leucodiatexitic host. The xenoliths have crenulate margins and a rim rich in biotite suggesting reaction with melt. (d) The RLS–country rock contact. The marginal norites are brecciated and invaded by leucosome.

Discordant leucosomes commonly occur above antiformal closures of folded quartz–sillimanite veins (Fig. 2a and c), suggesting a genetic relationship. Although discordant leucosomes appear undeformed, they commonly display a close geometric relation with the foliation (Fig. 2a and c) and, in particular, the fibrolite seams, which may be associated with leucosome-filled en echelon tension gash arrays (Fig. 2d). In some cases, discordant leucosomes, fibrolite seams and stromatic quartz–sillimanite veins form an interconnected network (diktyonitic structure; e.g. Fig. 2e) that is continuous on an outcrop scale. Such networks are more common at the Schwerin locality.

Higher-grade migmatites

At the Steelpoort dome locality, migmatites structurally ~100 m beneath the RLS contact are exposed in metapelitic rocks of the Vermont Formation (Hiemstra & Van Biljon, 1959; Fig. 1). At the Mokgorwane River locality, migmatized Lakenvalei Formation rocks are exposed in contact with the RLS (Fig. 1). Sedimentary structures are absent and the rocks are unfoliated.

The Vermont Formation rocks comprise two lithological varieties: massive leucosome-poor coarse-grained granofels, which contains abundant cordierite and conspicuous euhedral garnet porphyroblasts (Fig. 3a), and inhomogeneous diatexite (Fig. 3b). The granofels comprises a granulite-facies assemblage (e.g. Waters, 1988) of cordierite, biotite and garnet with minor plagioclase, ilmenite and quartz, and rare late white mica and chlorite, and contains thin (<10 mm wide) discontinuous veins and pods of leucosome (Fig. 3a). The grain-size distribution of garnet is bimodal. Larger grains (~10 mm) have near-perfect crystal faces and are mantled by a thin cordierite-rich layer; smaller euhedral grains (~1 mm) are concentrated within leucosome veins. Overall leucosome fractions are <5 vol. %. Although contact relations are poorly exposed, the garnetiferous rocks are bordered by inhomogeneous diatexite composed of cordierite, plagioclase, quartz, biotite, muscovite and rare, highly resorbed andalusite but no garnet; subrounded metasedimentary schollen are abundant (Fig. 3b).

In the Mokgorwane River, an ~50 m profile across the RLS–country rock contact zone is exposed. The rocks are characterized by leucodiatexite that comprises up to 90 vol. % leucosome in which occur subrounded schollen of metapsammite and calc-silicatefels and more angular xenoliths of medium- to fine-grained norite. Norite xenoliths have crenulate margins and distinct rims (<5 mm width) of coarse, decussate biotite (Fig. 3c). The leucodiatexite is composed of quartz, alkali feldspar and plagioclase; it contains abundant, subrounded quartz grains and wispy, subparallel trails of biotite. Further south, towards the RLS contact, the xenolith population becomes more angular and wholly noritic, and the proportion of leucosome decreases monotonically, suggesting that the leucodiatexite intruded and brecciated the marginal zone of the RLS (Fig. 3d).

MIGMATITE PETROGRAPHY

Lower-grade migmatites

Mesosome

The mesosome of the Silverton Formation migmatitic rocks exhibits different microstructural varieties that relate to variations in the fibrolite content of the rocks, principally the presence or absence of fibrolite seams. In fibrolite-deficient rocks, fine-scale bedding is preserved. The matrix contains subequal proportions of fabric-forming stubby biotite (0·1–0·5 mm) and granoblastic plagioclase and quartz (~0·1 mm; Fig. 4a). Clots of fibrolite within the matrix are rare and tourmaline is absent. Subhedral muscovite grains (<0·5 mm; Fig. 4a) cross-cut the foliation suggesting late (post-peak) growth. Plagioclase grains commonly show normal zoning (Fig. 4b). Euhedral to subhedral poikiloblasts of andalusite (commonly 1–2 mm), which are replaced around their margins by fine matted fibrolite (Fig. 4c), occur in Fe-richer rocks; cordierite forms anhedral, sieve-textured poikiloblasts up to 5 mm across in Mg-richer rocks.

In rocks where fibrolite is abundant (~1–10 vol. %), fine-scale bedding laminations are highly disrupted. Fibrolite occurs as isolated mats (Fig. 4d and e) and seams (e.g. Fig. 4f) that contain fibrolitized biotite and, commonly, skeletal ilmenite and/or titanomagnetite. The seams are up to 3 mm in width and are commonly subparallel to the foliation. Thin seams <1 mm across are discontinuous on a thin-section scale; larger examples may be continuous for many tens of centimetres or metres in outcrop (Fig. 2b). Matrix plagioclase grains are commonly larger and more strongly zoned than those in mesosome that lacks fibrolite seams.

Where fibrolite is abundant, irregular coarse-grained patches rich in quartz–plagioclase–fibrolite- and/or muscovite–fibrolite are abundant; we refer to these as leucocratic patches. Leucocratic patches are associated with corroded and fibrolitized andalusite poikiloblasts in Fe-richer rocks (Fig. 4d and e). Leucocratic patches are equally abundant within more magnesian andalusite-free rocks (Fig. 4f and g). The leucocratic patches are up to a few millimetres across and, although irregular, generally have long axes aligned subparallel to the foliation.

Where in contact with the finer-grained matrix, the patches are irregular and cuspate and exhibit low dihedral angles against matrix phases (see Laporte *et al.*, 1994; Laporte, 1997). Quartz- and/or plagioclase-dominated leucocratic patches comprise mosaics of highly sutured grains (~0·5 mm) and contain small (<0·1 mm) euhedral, inclusion-free, commonly pinitized cordierite (Fig. 4e and f). Some patches comprise anhedral muscovite enclosing euhedral cordierite (Fig. 4g). Examples containing quartz, plagioclase and muscovite are present. Larger (greater than or much greater than 1 mm), anhedral poikiloblasts of matrix cordierite are clearly distinct from cordierite within the leucocratic patches. The leucocratic patches are intimately related to discontinuous fibrolite mats and more continuous seams that splay into and terminate within the patches (Fig. 4d–g).

Leucocratic patches and fibrolite (>10 vol. %) are most abundant in tourmaline-bearing mesosome where no evidence of former bedding is preserved. In these examples, leucocratic patches contain small (<0·2 mm) euhedral tourmaline (± cordierite). Corroded fragments of andalusite are rare. Residual areas are composed of abundant biotite and fibrolite and larger (<1 mm) grains of tourmaline and decussate chlorite (<2 mm) that cross-cut the foliation. Plagioclase is uncommon although euhedral grains associated with interstitial, cuspate quartz and coarse muscovite may be locally abundant (Fig. 4h). Subrounded fragments of mesosome ~1·0 mm across are common and comprise subequal proportions of biotite quartz and plagioclase. Areas rich in leucocratic patches may grade into quartz–sillimanite veins and/or discordant leucosomes.

Quartz–sillimanite veins

Stromatic quartz–sillimanite veins comprise unstrained quartz (~1 mm) with anastomosing mats and seams of fibrolite and fibrolitized biotite that commonly include small ilmenite grains (Fig. 4i and j). Where present, plagioclase is commonly intergrown with quartz as coarse myrmekite (1–2 mm across); small accessory euhedral apatite and subrounded mesosome fragments are common. Away from small-scale folds, fibrolite defines a weak foliation that may be continuous from the mesosome and is at a low or moderate angle to bedding and the stromatic veins (Fig. 4i). In the cores of folds, the foliation is more strongly developed and steep to subvertical (Fig. 4j). Stromatic quartz–sillimanite veins are flanked by melanosome (1–3 mm) comprising biotite (~0·5 mm), fibrolitic sillimanite and opaque phases (<0·2 mm; Fig. 4i). The veins may grade into coarser-grained discordant quartzofeldpathic leucosome, particularly around ptygmatic fold hinges (e.g. Fig. 2a).

Discordant leucosome

Within discordant leucosome, quartz, plagioclase (~2–3 mm) and decussate muscovite (up to 10 mm)

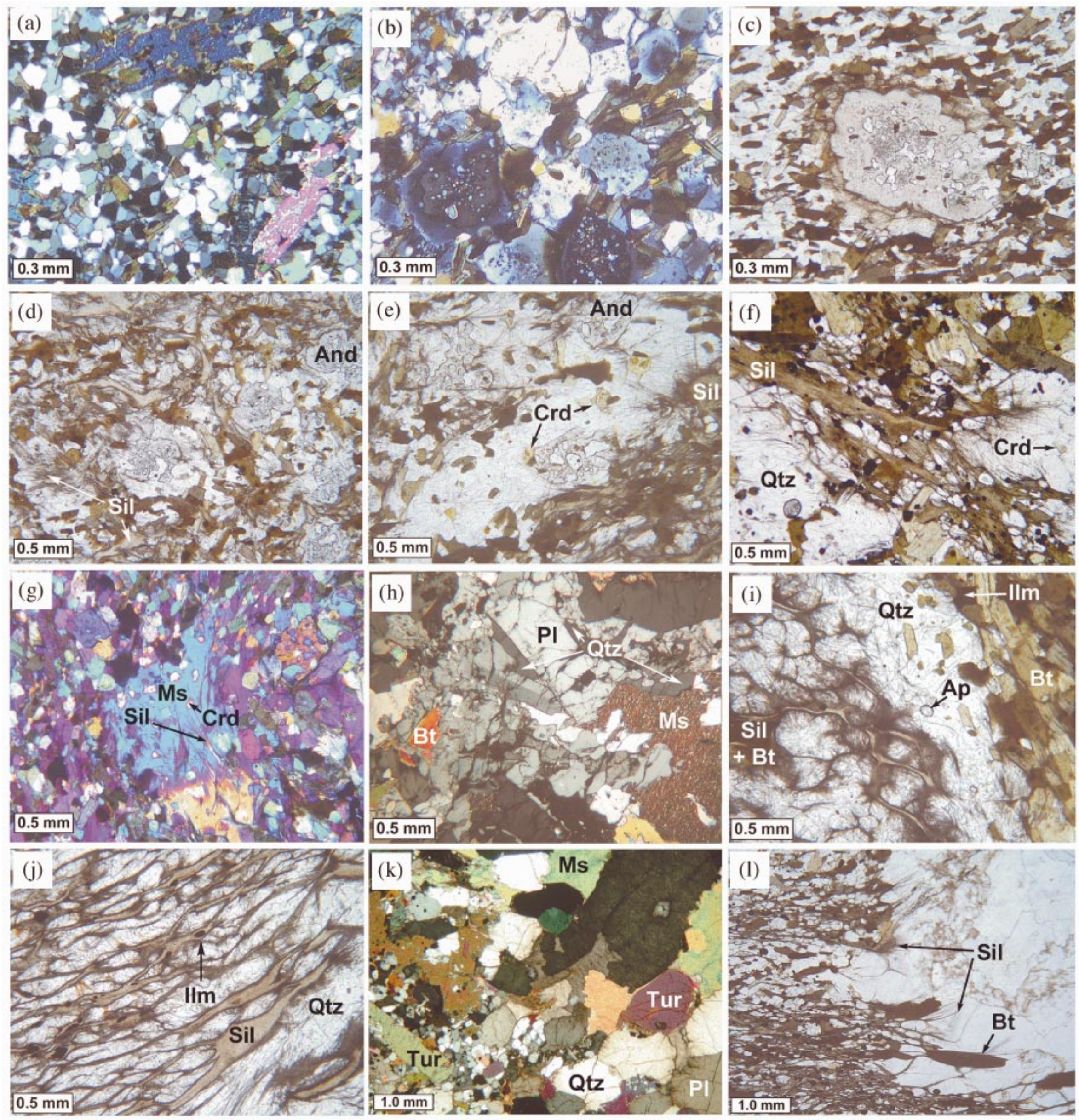

Fig. 4. Petrography of lower-grade migmatites. (a) Coarse muscovite plates cross-cutting the matrix and weak foliation; in these examples the muscovite is interpreted to represent post-peak subsolidus growth. (b) Normal zoning within matrix plagioclase grains. The compositional zoning is more strongly developed and grains tend to be coarser in rocks that are interpreted to have contained a greater melt fraction. (c) Andalusite poikiloblasts in Fe-richer metapelitic rocks show marginal replacement by fibrolitic sillimanite. (d) Early stage of leucocratic patch formation in Fe-richer rocks. The patches, interpreted to pseudomorph melt pockets, nucleate around corroded reactant andalusite. Discontinuous fibrolite mats (Sil) are common. (e) In stages where higher degrees of melting are inferred, the leucocratic patches form millimetric segregations that are associated with pinitized peritectic cordierite. Internal structures within the mesosome have been destroyed. Discontinuous mats and seams of fibrolite splay into the patches from the proximal mesosome, suggesting limited H_2O-fluxed melting. (f) Quartzofeldpathic patches containing pinitized peritectic cordierite within more magnesian (andalusite-free) metapelites. The fibrolite seam, which terminates and splays into the patch, should be noted. (g) Muscovite-dominated patch associated with fibrolite seams and pinitized cordierite. (Crossed polars with one-wave tint plate inserted.) (h) Plagioclase accumulation within leucosome-rich mesosome. The euhedral form of the plagioclase and the interstitial, cuspate quartz suggests former melt presence. (i) Stromatic quartz–sillimanite vein (QSV) that contains abundant fibrolitized biotite and rare euhedral apatite. Fibrolite defines a weak foliation that is at a low angle to the vein margin. The residual biotite-rich melanosome in which ilmenite (Ilm) grains are concentrated should be noted (right). (j) Within the cores of small-scale, ptygmatic folds in QSVs, a strong, fibrolite- and fibrolitized biotite-defined, subvertial axial planar schistosity is developed. (k) Coarse-grained discordant leucosome. These bodies have granitic compositions [Qtz, Pl, Ms (after Kfs?)], are undeformed and are rich in coarse tourmaline and biotite. Small inclusions of fibrolite are ubiquitous. (Crossed polars.) (l) Coarse-grained discordant leucosome (right) and mesosome (left). The numerous foliation-parallel fibrolite seams that terminate and splay into the leucosome suggest that discordant leucosomes were the result of H_2O-fluxed melting. Mineral abbreviations follow Kretz (1983).

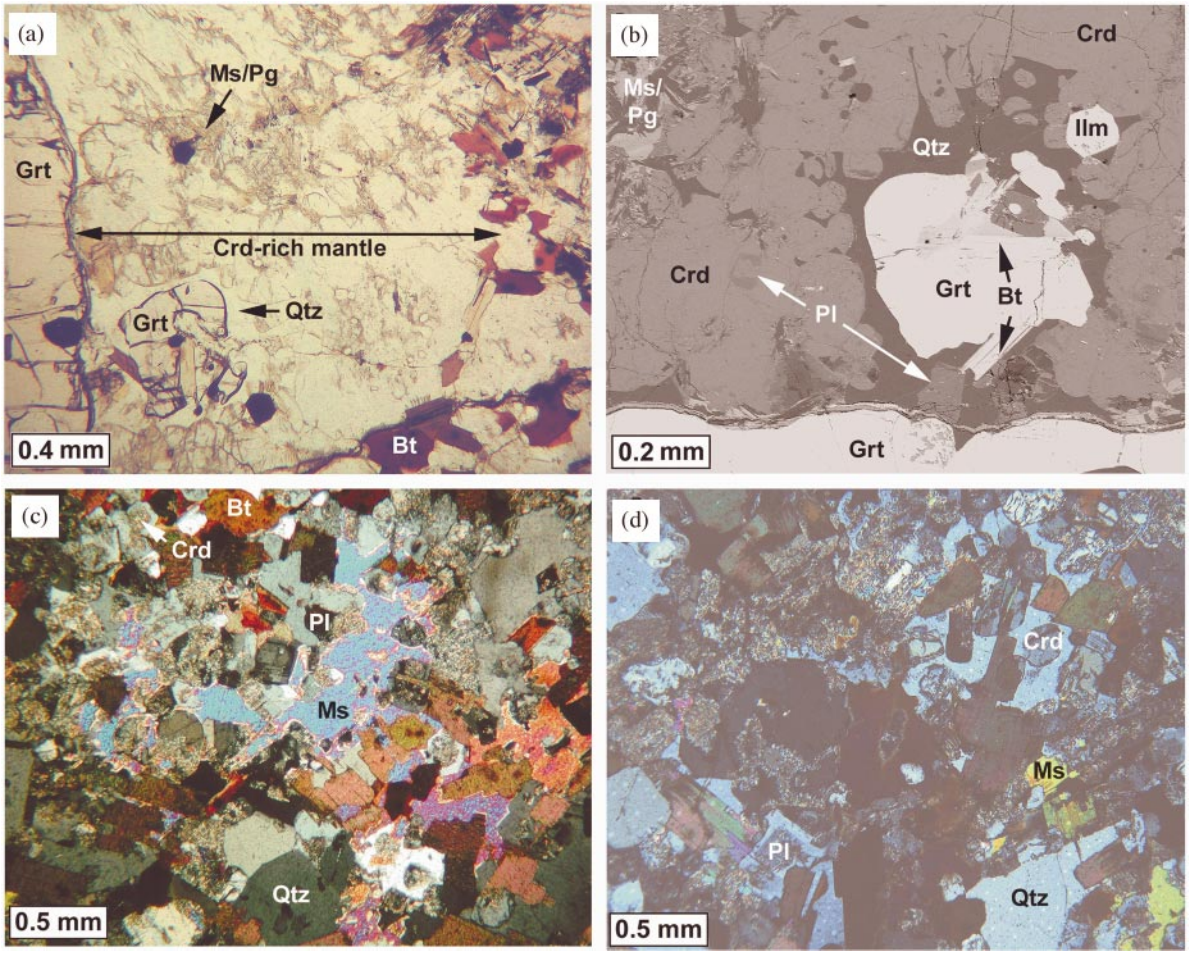

Fig. 5. Petrography of higher-grade migmatites. (a) Plane-polarized light image of granofels showing cordierite-rich mantle separating large garnet (left) from the biotite–cordierite-rich matrix (right). (b) Back-scattered image of the mantle surrounding a large ~10 mm garnet (bottom). The mantle comprises a crystal-supported framework dominated by euhedral cordierite with minor normally zoned plagioclase, decussate white mica and ilmenite; extreme melt loss is implied. The area surrounding the small garnet is characterized by an optically continuous cuspate patch of interstitial quartz, which is interpreted to pseudomorph melt. (c) and (d), inhomogeneous schollen diatexite containing abundant cuspate, interstitial grains of muscovite, quartz and feldspar that are interpreted to pseudomorph melt. The matrix is dominantly leucosome supported and is rich in hydrous phases and/or alteration products.

form large irregular grains that are commonly intergrown. At the Monaps locality, these may exhibit cauliform margins (Fig. 4k). Subhedral biotite up to 5 mm across is distinct from finer-grained matrix biotite in mesosome. Although generally absent, rare cordierite occurs as large (up to 3 mm) euhedral, inclusion-free grains that commonly exhibit ragged, pinitized margins. Small euhedral tourmaline (1–2 mm) is abundant. Ubiquitous anastomosing fibrolite seams can be traced from the mesosome into the coarse discordant leucosome into which they splay and terminate (Fig. 4l). Randomly orientated inclusions of fibrolite (< 0·05 mm) are common within all phases other than tourmaline.

Higher-grade migmatites

Garnet granofels

The matrix of the leucosome-poor Vermont Formation granofels comprises a broadly equigranular (~0·5 mm) mosaic of euhedral to subhedral cordierite and randomly orientated biotite with minor plagioclase and ilmenite. Large (~10 mm across) euhedral garnet grains contain inclusions of rounded quartz and stubby ilmenite. Biotite rarely occurs within fractures and as coarse flakes at the margins of garnet. Large garnets are surrounded by a mantle (0·5–2·0 mm in width) comprising euhedral, slightly pinitized cordierite (up to 1 mm across) and rare normally zoned plagioclase (~0·1 mm) that form a touching, apparently crystal-supported framework (Fig. 5b). Quartz forms irregular, optically continuous patches that have pronounced cuspate margins with low dihedral angles against matrix phases (Fig. 5a and b). Irregular patches of white mica (Fig. 5a and b) and chloritized biotite occur within the mantle. More continuous leucosome veins (Fig. 3a) are up to 10 mm wide, lack melanosome and contain numerous euhedral, inclusion-free garnets (0·5–1·0 mm).

Inhomogeneous diatexite

The inhomogeneous diatexite comprises abundant normally zoned plagioclase with euhedral cores (~0·1 mm), euhedral (commonly altered) cordierite (up to 0·5 mm) that may be mantled by plagioclase, and randomly oriented coarse biotite (0·5–2 mm). Irregular, optically continuous, cuspate patches of interstitial muscovite (Fig. 5c), quartz (Fig. 5d) and feldspar, up to a few millimetres across, are abundant and enclose euhedral matrix phases. Matrix phases are commonly not in contact and the rock appears to have a leucosome-supported framework.

Leucodiatexite

The leucosome-rich rock hosting the brecciated norite xenoliths within the Mokgorwane River is deficient in mafic phases and has a typical granitic microstructure and composition, comprising subequal quantities of anhedral quartz and alkali feldspar (both microcline and micro/meso-perthite) with minor plagioclase (~5 vol. %). Ragged chloritized biotite (up to 1 mm) and small, pinitized cordierite are rare (<0·2 mm). Rounded quartz grains up to 20 mm in diameter are abundant.

MINERAL CHEMISTRY

Compositional data were obtained using the JEOL JXA-8900 SuperProbe at the Center for Microanalysis and Microscopy, University of Maryland. Operating conditions for spot analyses were 15 kV and 20 nA; spot sizes were 5–10 μm depending on the analysed phase. Natural materials were used as standards. Representative analyses are given in Tables 1–3. Mineral abbreviations follow Kretz (1983).

Garnet

Both generations of garnet within the granofels (BV-114) are almandine rich and compositionally similar. Large garnets are broadly homogeneous and have $X_{Alm}^{Grt} = 0{\cdot}76$–$0{\cdot}77$ [where $X_{Alm}^{Grt} = Fe^{2+}/(Fe^{2+} + Mg + Ca + Mn]$, $X_{Prp}^{Grt} = 0{\cdot}16$–$0{\cdot}14$ and X_{Mg} [Mg/$(Fe^{2+} + Mg)$] of 0·16–0·17. Spessartine and grossular concentrations are constant at 4–5 mol %. At the extreme edges of grains (within ~100 μm) and around marginal biotite inclusions and biotite-filled fractures, almandine contents are higher $X_{Alm}^{Grt} \sim 0{\cdot}82$); pyrope contents are similarly reduced and grossular may be higher, and spessartine lower, by up to 1 mol %. Small garnets within leucosome veins have uniform compositions ($X_{Alm}^{Grt} = 0{\cdot}77$) except for thin retrograde rims ($X_{Alm}^{Grt} = 0{\cdot}80$).

Cordierite

Cordierite within leucocratic patches from the metatexites at the Monaps locality (BV-51) is largely unzoned with $X_{Mg} = 0{\cdot}70$–$0{\cdot}75$. Inclusions within muscovite may have lower X_{Mg} (~0·60). Concentrations of the Mn-cordierite component are 3–4 mol % and Na contents are ~0·10–0·12 c.p.f.u. (18 O). Cordierite from samples at the Schwerin locality (BV-27, BV-28) has $X_{Mg} = 0{\cdot}58$–$0{\cdot}62$. Large cordierite grains within discordant leucosome have $X_{Mg} = 0{\cdot}55$–$0{\cdot}57$, and marginally lower concentrations of the Mn end-member (1–2 mol %) and Na (0·08–0·09 c.p.f.u.).

Within the garnet granofels and inhomogeneous diatexite (BV-110), variations in cordierite compositions are slight. Cores ($X_{Mg} = 0{\cdot}56$–$0{\cdot}60$) may be marginally more magnesian than rims ($X_{Mg} = 0{\cdot}55$–$0{\cdot}58$), although the reverse occurs. Mn-cordierite concentrations are low (~0·5 mol %); slightly higher values (1·5–2·0 mol %) are recorded in the diatexite. Na contents are in the range 0·02–0·08 c.p.f.u.

Biotite

At the Monaps locality, mesosome biotite has $X_{Mg} = 0{\cdot}49$–$0{\cdot}52$ and octahedral Al contents ($X_{Al,M1}$) of 0·45–0·50 c.p.f.u. (11 O); at Schwerin, biotite is less magnesian ($X_{Mg} = 0{\cdot}35$–$0{\cdot}40$) and Al enriched ($X_{Al,M1} = 0{\cdot}50$–$0{\cdot}55$). TiO_2 contents are 1·5–2·0 wt % and 1·2–2·5 wt %, respectively. K/Na ratios (0·92–0·95) and concentrations of CaO (<0·1 wt %) and MnO (0·2–0·3 wt %) are similar throughout. There is no significant difference in the composition of biotite within leucosome, mesosome and melanosome.

In the granofels, biotite from the matrix, within leucosome veins and replacing garnet is compositionally similar. X_{Mg} varies from 0·39 to 0·45, TiO_2 contents are 2·2–3·3 wt % and $X_{Al,M1}$ concentrations are 0·30–0·40 c.p.f.u. (11 O). K/Na ratios are 0·96–0·98. MnO and CaO concentrations are low (~0·05 and <0·03 wt %, respectively). There is no systematic change in biotite composition with increasing distance from large garnets. Within the neighbouring inhomogeneous diatexite, biotite is enriched in Fe ($X_{Mg} = 0{\cdot}33$–$0{\cdot}38$), K (K/Na = 0·98–0·99), Al

Table 1: Representative analyses of garnet and cordierite

Phase:	Garnet					Cordierite					
Sample:	BV-114 (large Grt)			BV-114 (small Grt)		BV-51	BV-27	BV-28	BV-110	BV-114	
Position:	core	int.	rim	core	rim	LP	LP	DL	matrix	matrix	leuco.
SiO_2	36·84	37·52	37·16	36·96	37·26	48·64	48·18	48·02	47·80	48·55	48·27
TiO_2	0·00	0·04	0·01	0·02	0·04	0·03	0·02	0·03	0·00	0·00	0·00
Al_2O_3	21·08	21·12	20·96	20·91	20·74	33·25	33·03	33·08	32·77	33·06	32·93
Fe_2O_3	1·42	0·63	0·80	1·00	0·06	1·50	2·03	2·09	1·56	1·50	1·09
FeO	33·60	34·74	36·28	34·05	35·87	5·41	7·30	9·18	9·42	9·50	9·50
MnO	1·93	1·77	1·40	1·52	1·40	0·65	0·65	0·30	0·40	0·13	0·10
MgO	3·71	3·66	2·53	3·73	2·92	8·16	6·73	6·30	6·62	7·03	7·13
CaO	1·48	1·43	1·73	1·55	1·63	0·05	0·02	0·02	0·00	0·00	0·00
Na_2O	n.a.	n.a.	n.a.	n.a.	n.a.	0·64	0·63	0·40	0·20	0·18	0·12
K_2O	n.a.	n.a.	n.a.	n.a.	n.a.	0·00	0·00	0·02	0·00	0·00	0·00
Total	100·05	100·92	100·88	99·74	99·93	98·34	98·60	99·43	98·78	99·95	99·15
Formula	*8C*	*8C*	*8C*	*8C*	*8C*	*18O*	*18O*	*18O*	*18O*	*18O*	*18O*
Si	2·959	2·987	2·983	2·976	3·008	4·982	4·972	4·948	4·956	4·967	4·971
Ti	0·000	0·002	0·000	0·001	0·003	0·002	0·002	0·002	0·000	0·000	0·000
Al	1·996	1·983	1·984	1·985	1·974	4·015	4·019	4·018	4·006	3·987	3·998
Fe^{3+}	0·086	0·038	0·049	0·060	0·004	0·116	0·157	0·162	0·122	0·115	0·084
Fe^{2+}	2·257	2·313	2·436	2·293	2·422	0·463	0·630	0·791	0·817	0·813	0·818
Mn	0·131	0·119	0·095	0·104	0·095	0·057	0·057	0·026	0·035	0·011	0·009
Mg	0·444	0·435	0·303	0·447	0·352	1·246	1·035	0·967	1·023	1·072	1·095
Ca	0·127	0·122	0·149	0·134	0·141	0·005	0·002	0·002	0·000	0·000	0·000
Na	—	—	0·000	—	—	0·128	0·127	0·080	0·041	0·036	0·024
K	—	—	0·000	—	—	0·000	0·000	0·002	0·000	0·000	0·000
Sum	8·000	8·000	8·000	8·000	8·000	11·014	11·001	11·000	11·000	11·000	11·000
X_{Mg}	0·16	0·16	0·11	0·16	0·13	0·73	0·62	0·55	0·56	0·57	0·57

LP, leucocratic patch; DL, discordant leucosome; *nC*, number of cations; *nO*, number of oxygens. n.a., not analysed.

($X_{Al,M1}$ ~0·40–0·50 c.p.f.u.) and Mn (MnO ~0·15 wt %). F contents are highest in the granofels (>0·20 wt %); Cl contents are highest in the inhomogeneous diatexite (0·50–0·80 wt %).

White mica

At lower grades, white mica is muscovite rich ($X_{Ms}^{W.Mica} = 0·83–0·94$) and contains little or no Ca ($\ll 1$ mol % margarite). Muscovite within leucocratic patches is more phengitic (~0·2 c.p.f.u. Fe; 11 O); larger grains within discordant leucosome are Fe poor. Patches of intergrown, radiating white mica clusters within the garnet granofels range from muscovite rich ($X_{Ms}^{W.Mica} = 0·65–0·80$) to paragonite rich ($X_{Ms}^{W.Mica} = 0·80–0·85$). Margarite concentrations are up to 6 mol %. Within the inhomogeneous diatexite, white mica is muscovite rich ($X_{Ms}^{W.Mica} = 0·90–0·91$); margarite comprises <1 mol %. Total Fe oxide contents in white mica from higher-grade rocks are up to 1 wt %.

Feldspar

Matrix plagioclase in mesosome of metatexites at both the Monaps and Schwerin localities has euhedral to subhedral andesine–oligoclase cores ($X_{An}^{Pl} = 0·20–0·30$) and oligoclase rims ($X_{An}^{Pl} = 0·14–0·18$). Orthoclase contents are up to 1 mol % and Fe contents are low (<0·3 wt % as oxides). Plagioclase within quartz–sillimanite veins, leucocratic patches and discordant leucosomes is compositionally similar to that within the matrix but commonly shows patchy zonation.

Table 2: Representative analyses of biotite

Phase:	Biotite					
Sample:	BV-51	BV-27		BV-110	BV-114	
Position:	matrix	matrix	DL	matrix	matrix	leuco.
SiO_2	36·99	36·05	35·73	34·51	35·76	35·08
TiO_2	1·91	1·74	2·38	4·02	2·55	2·94
Al_2O_3	19·79	20·78	20·53	19·47	19·28	18·79
Fe_2O_3	0·00	0·00	0·00	0·00	0·45	0·00
FeO	18·34	21·27	21·81	22·38	22·27	21·47
MnO	0·25	0·23	0·19	0·15	0·04	0·01
MgO	10·10	8·01	7·15	6·61	8·53	8·44
CaO	0·00	0·00	0·00	0·00	0·00	0·00
Na_2O	0·35	0·33	0·44	0·08	0·18	0·18
K_2O	8·70	8·43	8·48	8·92	8·38	8·64
F	0·15	0·15	0·19	0·14	0·28	0·22
Cl	0·02	0·02	0·00	0·72	0·09	0·10
$O^- \equiv F + Cl$	0·07	0·07	0·08	0·21	0·18	0·13
Total	96·35	96·77	96·63	95·93	97·26	95·43
Formula	*11O*	*11O*	*11O*	*11O*	*11O*	*11O*
Si	2·743	2·696	2·687	2·637	2·678	2·679
Ti	0·106	0·098	0·135	0·231	0·144	0·169
Al	1·730	1·833	1·821	1·754	1·703	1·692
Fe^{3+}	0·000	0·000	0·000	0·000	0·025	0·000
Fe^{2+}	1·137	1·330	1·372	1·430	1·395	1·371
Mn	0·016	0·015	0·012	0·009	0·002	0·001
Mg	1·116	0·893	0·801	0·753	0·952	0·961
Ca	0·000	0·000	0·000	0·000	0·000	0·000
Na	0·050	0·047	0·064	0·011	0·027	0·027
K	0·824	0·805	0·814	0·870	0·802	0·842
F	0·057	0·059	0·074	0·056	0·110	0·090
Cl	0·003	0·005	0·000	0·150	0·091	0·022
Sum	7·782	7·781	7·780	7·901	7·929	7·854
X_{Mg}	0·50	0·40	0·37	0·34	0·41	0·41

DL, discordant leucosome.

Within the granofels, matrix and leucosome plagioclase has euhedral, bytownite cores ($X^{Pl}_{An} = 0·75–0·77$) and andesine–labradorite rims ($X^{Pl}_{An} = 0·43–0·53$). Orthoclase concentrations are <0·5 mol % and <0·1 mol %, respectively. Ferric iron contents are <0·4 wt %. Plagioclase in the inhomogeneous diatexite is significantly more albitic; oligoclase rims ($X^{Pl}_{An} = 0·13–0·18$) surround euhedral andesine cores ($X^{Pl}_{An} = 0·32–0·44$). Plagioclase mantling cordierite is andesine. Orthoclase contents are <1 mol % and Fe_2O_3 contents <0·2 wt %.

Plagioclase grains within the homogeneous leucodiatexite (BV-127) are largely unzoned although different grains vary in composition ($X^{Pl}_{An} = 0·30–0·40$). Orthoclase contents are <1 mol % and iron contents negligible. Alkali feldpar comprises orthoclase-rich grains ($X^{Kfs}_{Or} = 0·80–0·90$, $X^{Kfs}_{Or} < 0·01$) with fine Na-rich exsolution lamellae ($X^{Kfs}_{Or} \sim 0·25$, $X^{Kfs}_{Or} < 0·03$).

Thermobarometry

Constraints on peak $P–T$ conditions were obtained from multi-equilibria calculations using the Holland & Powell (1998; updated 19/09/99) dataset. The process involves inputting the activities of the end-members of the inferred stable phases (calculated from mineral chemistry using the program AX—see http://www.esc.cam.ac.uk/astaff/holland/ax.html). The output consists of numerous dependent reactions, of which an (arbitrary) independent set is used to constrain $P–T$. In the higher-grade rocks, garnet exhibits limited compositional zoning except at the extreme rims; core compositions (high X_{Mg}) were used in the calculations. In all rocks, plagioclase cores are richest in the An component, consistent with equilibration at T_{max}. Other phases show little compositional variation. In lower-grade rocks biotite distal from cordierite was chosen to minimize the effect of any retrograde Fe–Mg exchange. Phases inferred to have developed by retrograde reaction (i.e. muscovite, chlorite) were not included.

The combined results suggest pressures of ~3·5 ± 1·5 kbar. These results are consistent with, but less well constrained than, the 3·0 ± 0·5 kbar results of Waters & Lovegrove (2002). In the garnet granofels, garnet–cordierite Fe–Mg thermometry using the Holland & Powell (1998) dataset gives ~750 ± 100°C. The amount of Na within cordierite decreases as the contact is approached, consistent with rising T (Mirwald, 1986; Kalt *et al.*, 1998). Concentrations of ~0·10 c.p.f.u. Na (18 O) in the metatexites at lower grades suggest 600–650°C; higher T (650–800°C) is recorded by the granofels and the inhomogeneous diatexite (Na = 0·02–0·08 c.p.f.u.).

METAMORPHIC EVOLUTION

Thermal considerations

Cawthorn & Walraven (1998) modelled the emplacement of the RLS as a series of magma pulses and inferred from the limited degree of differentiation that the entire suite, conservatively estimated at 370 000–600 000 km^3 of magma (Cawthorn & Walraven, 1998), was emplaced within 75 kyr. To a first approximation, the thermal structure of the floor rocks can be modelled by considering a single thermal pulse at a pressure reflecting the overburden that includes the full

Table 3: Representative analyses of plagioclase

Phase:	Plagioclase									
Sample:	BV-51		BV-27		BV-28	BV-110		BV-114		BV-127
Position:	core	rim	core	rim	DL	core	rim	core	rim	
SiO_2	62·00	64·52	61·53	63·66	62·97	56·33	64·04	48·19	55·25	59·96
TiO_2	0·00	0·01	0·02	0·00	0·00	0·03	0·00	0·00	0·04	0·02
Al_2O_3	24·52	23·08	24·11	22·95	22·98	27·85	22·72	32·83	28·02	25·59
Fe_2O_3	0·13	0·25	0·04	0·01	0·02	0·05	0·15	0·17	0·25	0·02
FeO	0·00	0·00	0·00	0·00	0·00	0·00	0·00	0·00	0·00	0·00
MnO	0·01	0·02	0·00	0·00	0·00	0·02	0·00	0·00	0·01	0·03
MgO	0·00	0·00	0·00	0·04	0·00	0·00	0·00	0·00	0·00	0·00
CaO	5·36	3·29	5·25	3·53	3·98	9·02	3·24	15·80	10·33	6·58
Na_2O	8·65	9·82	8·48	9·69	9·12	6·28	9·71	2·51	5·70	7·91
K_2O	0·07	0·05	0·14	0·07	0·07	0·10	0·12	0·03	0·06	0·11
Total	100·72	101·05	99·57	99·94	99·14	99·67	99·99	99·52	99·67	100·21
Formula	*8O*	*8O*	*8O*	*8O*	*8O*	*8O*	*8O*	*8O*	*8O*	*8O*
Si	2·730	2·817	2·739	2·811	2·802	2·534	2·824	2·215	2·496	2·664
Ti	0·000	0·000	0·001	0·000	0·000	0·001	0·000	0·000	0·002	0·001
Al	1·273	1·188	1·265	1·194	1·206	1·477	1·181	1·780	1·493	1·341
Fe^{3+}	0·004	0·008	0·001	0·000	0·001	0·002	0·005	0·006	0·009	0·001
Fe^{2+}	0·000	0·000	0·000	0·000	0·000	0·000	0·000	0·000	0·000	0·000
Mn	0·000	0·001	0·000	0·000	0·000	0·001	0·000	0·000	0·000	0·001
Mg	0·000	0·000	0·000	0·003	0·000	0·000	0·000	0·000	0·000	0·000
Ca	0·253	0·154	0·250	0·167	0·190	0·435	0·153	0·778	0·500	0·313
Na	0·738	0·831	0·732	0·829	0·787	0·548	0·831	0·224	0·499	0·681
K	0·004	0·003	0·008	0·004	0·004	0·006	0·007	0·002	0·004	0·006
Sum	5·002	5·002	4·997	5·009	4·990	5·002	5·001	5·004	5·003	5·008
X_{An}	0·25	0·16	0·25	0·17	0·19	0·44	0·15	0·77	0·50	0·31

DL, discordant leucosome.

thickness of the RLS (Waters & Lovegrove, 2002). Rocks at successively deeper levels would have attained progressively lower T_{max} at progressively later times.

The simplified model presented here considers a sill of magma of 7 km thickness with an initial T of 1300°C (Cawthorn & Walraven, 1998), emplaced into a sedimentary pile at a depth of 3 km with a normal crustal geotherm of 25°C/km. Thermal diffusivity is taken as 10^{-6} m^2/s. An additional thermal input into the floor rocks, nominally taken as 100°C, accounts for a small degree of heating associated with the locally abundant pre- and syn-Bushveld sills (e.g. Sharpe & Hulbert, 1985). The effects of heat transport by fluid advection are regarded as negligible (see Connolly & Thompson, 1989) and, despite the likelihood of convective cooling in the RLS magma chamber, it is probable that the aureole rocks were rapidly isolated from the magma by crystal accumulation on the chamber floor. For these reasons, we consider only conductive heating in the model.

Figure 6 shows the distribution of T with time for rocks at different distances from the RLS contact. At pressures of ~3 kbar, rocks within 750 m of the contact are predicted to be at T in excess of the H_2O-saturated granite solidus (e.g. Johannes, 1984; Ebadi & Johannes, 1991; Holland & Powell, 2001) and the model metapelite solidus (e.g. White *et al.*, 2001). The lower-grade migmatites discussed here are ~300–350 m beneath the contact, where a peak T of ~680–690°C is predicted ~150 kyr after intrusion. Only rocks within ~100 m of the RLS are predicted to have attained $T \geq 725$°C, conditions under which garnet-producing volatile-phase-absent melting occurs (e.g. Le Breton & Thompson, 1988; Johnson *et al.*, 2001*b*; White *et al.*, 2001). Analogous outcrops on the

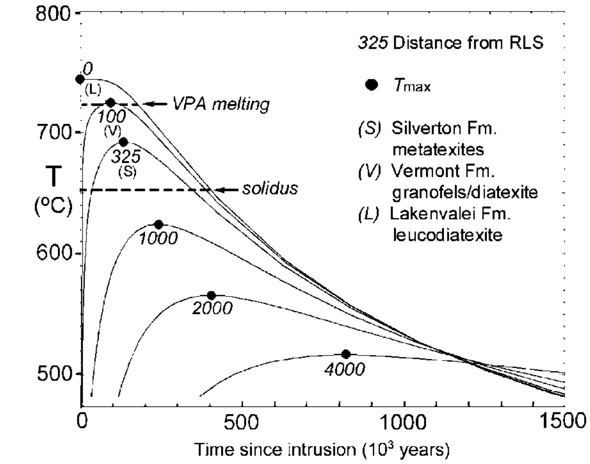

Fig. 6. Simple 1-D conductive heating model showing the distribution of T with time for rocks in the Bushveld aureole. The curves denote various distances below the contact, which relate to the outcrops discussed in the text. The T values of the metapelite solidus and the onset of major melt production via volatile-phase-absent (VPA) melting consuming biotite are shown. Isochrons (which would be vertical lines in the figure) indicate that an inverted geothermal gradient existed for >1 Myr after intrusion.

margins of the Steelpoort dome are predicted to have reached $T_{max} \sim 75$ kyr after intrusion. The predicted T at the RLS–country rock interface of ~750°C is sufficiently high for production of peritectic orthopyroxene (e.g. White *et al.*, 2001).

The thermal model is undoubtedly a simplification, i.e. it does not account for exothermic heat of fusion from the crystallizing RLS or endothermic reactions in the aureole rocks. However, the modelled profile correlates well with the observed outer limit of leucosome development (the migmatite front) and the spatial development of garnet- and orthopyroxene-bearing migmatites. The predicted T of ~500°C in rocks ~4 km from the contact is in good agreement with results of garnet–biotite Fe–Mg exchange thermometry reported by Waters & Lovegrove (2002). The predicted T at the contact (~750°C) is consistent with the estimates (760°C) of Engelbrecht (1990) and data herein.

Modelling phase relations

We have modelled phase relations in the NCKFMASH system using THERMOCALC v. 3.1 (Powell & Holland, 1988) and the Holland & Powell (1998; updated 19/09/99) dataset. Melts were modelled on an eight-oxygen basis following White *et al.* (2001). The coding for all phases, including regular solution interaction parameters to account for non-ideality, follows White *et al.* (2001). All software and data files are available at http://www.esc.cam.ac.uk/astaff/holland/thermocalc.html.

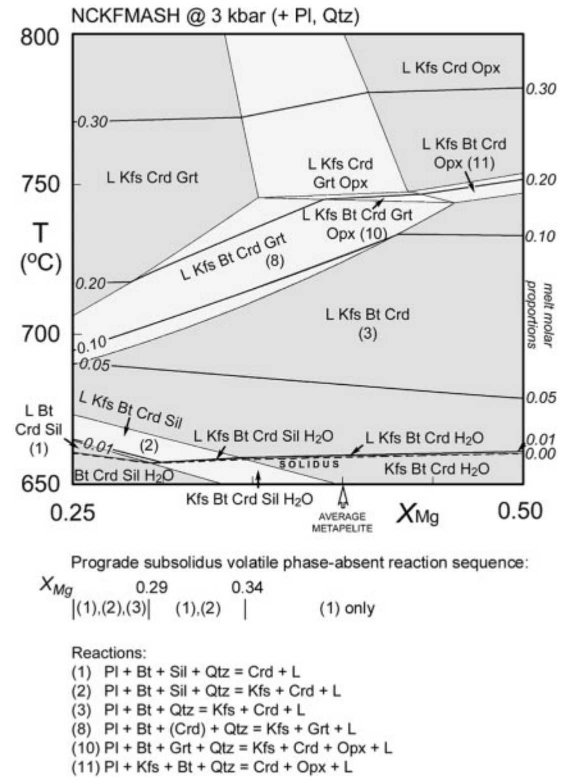

Fig. 7. T–X_{Mg} pseudosection based on the mean metapelite composition. The amount of H_2O is just enough to saturate the solidus at the Fe-rich edge, artificially lowering the melt mode isopleths to lower T with increasing X_{Mg}. The white arrow shows the X_{Mg} (0·40) of the mean metapelite composition. Reactions that occur across the multivariant fields (in parentheses) are in an up-T sense. The depth of shading reflects increasing variance; the darkest fields are quadrivariant. The normalized bulk composition (in mol %) of the left- and right-hand edges of the diagram in terms of the components H_2O:SiO_2:Al_2O_3:CaO:MgO:FeO:K_2O:Na_2O are 5·21:64·21:13·27:0·54:3·38:10·14:2·08:1·16 and 5·21:64·21:13·27:0·54:6·77:6·76:2·08:1·16, respectively.

The well-constrained aureole pressure of ~3 kbar allows investigation of phase relations using T–X pseudosections (Figs 7–10) that are calculated for an 'average' Pretoria Group metapelite bulk composition, derived from the mean composition of 15 bulk-rock samples of Silverton Formation metapelitic rocks. The primary compositional variations controlling the paragenetic evolution of the rocks considered here are: (1) X_{Mg}, which shows a bulk increase towards stratigraphically higher levels (Waters & Lovegrove, 2002) as well as variability within individual outcrops; (2) variable H_2O (T–X_{H_2O}), important in assessing the contribution of any volatiles potentially derived from underlying dehydrating rocks; (3) variable melt loss or melt gain (T–X_{melt}), important in examining the efficacy of melt extraction and preservation of peak metamorphic assemblages (White & Powell, 2002). The reported upward bulk increase in Na and Ca in

Pretoria Group rocks will result in an increase in modal plagioclase (Waters & Lovegrove, 2002), but should have little effect on phase relations and is not considered here.

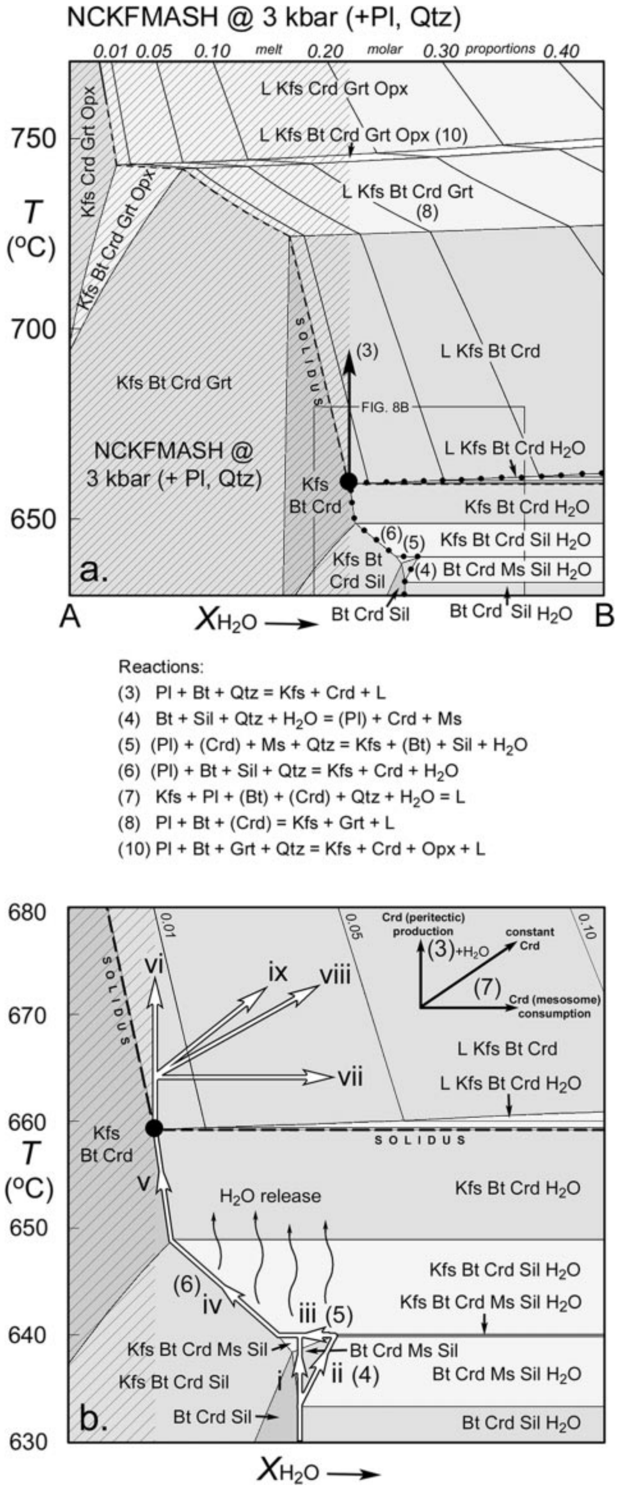

Net reactions within and across polyvariant fields [reactions (1)–(11)] were determined by comparing the calculated modal proportions of phases at higher T with those at lower T. Those phases that showed an increase in modal abundance with rising T were inferred to have been reaction products, whereas those that decreased in abundance were inferred to have been reactants. The T–X pseudosections were calculated with no phase in excess although plagioclase and quartz are predicted in all assemblages at the P–T of interest. In THERMOCALC, phase proportions are calculated on a one-oxygen basis; consequently, mol % can be generally taken to approximate vol. %.

Around the metamorphic peak for rocks in the inner aureole, T dropped with increasing depth (Fig. 6) and the T–X pseudosections approximate a vertical section through the aureole; a T variation of 50°C is equivalent to a stratigraphic thickness of around 350 m.

Lower-grade migmatites

Figure 7 shows a T–X_{Mg} pseudosection at 3 kbar based on the mean metapelite composition with no excess H_2O above that required to saturate the solidus. The variation in X_{Mg} (0·25–0·50) is representative of the compositional range in Silverton Formation rocks. X_{Mg} exerts a strong control on aluminosilicate stability;

Fig. 8. (a) T–X_{H_2O} pseudosection based on the mean metapelite composition. The dotted line shows H_2O saturation ($a_{H_2O} = 1$). The normalized bulk composition of the left- and right-hand edges of the diagram in terms of the components H_2O:SiO_2:Al_2O_3:CaO:MgO:FeO:K_2O:Na_2O are 1·37:66·84:13·82:0·56:5·68:8·35:2·17:1·20 (X_{H_2O} = A) and 7·27:62·84:12·99:0·53:5·34:7·85:2·04:1·13 (X_{H_2O} = B), respectively. (b) Expanded area of Fig. 8 applicable to the lower-grade migmatites. The white arrows show the potential prograde paths, numbered segments [(i)–(ix)] of which are discussed in the text. The black arrows show vectors of changing cordierite proportions as suprasolidus reaction progresses. With no H_2O influx and a rise in T (vertical vector), peritectic cordierite is produced. With H_2O influx and no rise in T (horizontal vector), mesosome cordierite is consumed. The diagonal vector marks no change in the cordierite content. The length of the arrows marks a change of 0·25 mol % cordierite. The normalized bulk composition of the left- and right-hand edges of the diagram in terms of the components H_2O:SiO_2:Al_2O_3:CaO:MgO:FeO:K_2O:Na_2O are 4·10:64·99:13·44:0·55:5·52:8·12:2·11:1·17 and 6·37:63·46:13·12:0·53:5·39:7·93:2·06:1·14, respectively. The cross-hatched regions in (a) and (b) are not accessible; with all the H_2O locked up in hydrous phases (micas, cordierite and/or melt), lowering X_{H_2O} necessitates the removal of a proportion of one or more of these phases, thus removing components other than H_2O from the bulk composition for which the diagram is drawn. Numbers in parentheses refer to the reaction (discussed in the text) that occurs across the relevant multivariant field. The darkest fields are quinivariant.

only rocks more Fe rich than X_{Mg} of 0·34 contain sillimanite/andalusite at and above the solidus. Andalusite is abundant in Fe-richer migmatites of the study area, although its ubiquitous marginal alteration to fibrolite suggests andalusite was metastable with respect to sillimanite at peak T. The equilibrium model reactions consider only sillimanite as the stable Al_2SiO_5 polymorph.

At the T_{max} of interest for the lower-grade migmatites (~680–690°C; Fig. 6), melt proportions of ≤5 mol % are predicted (Fig. 7). Prograde volatile-phase-absent melting reactions for all bulk compositions produce a small volume of peritectic cordierite.

For Fe-richer rocks ($X_{Mg} < 0{\cdot}29$), melting proceeds via the following sequence of incongruent reactions:

$$\mathrm{Pl + Bt + Sil + Qtz \leftrightarrow Crd + L} \quad (1)$$

$$\mathrm{Pl + Bt + Sil + Qtz \leftrightarrow Kfs + Crd + L} \quad (2)$$

$$\mathrm{Pl + Bt + Qtz \leftrightarrow Kfs + Crd + L.} \quad (3)$$

For rocks with intermediate X_{Mg} (~0·29–0·34), reaction (2) is seen at the solidus, whereas for rocks with $X_{Mg} > 0{\cdot}34$, reaction (3) is the volatile-phase-absent equilibrium seen at the solidus (Fig. 7). The aluminium required for product cordierite generated by reaction (3) is derived from biotite, which becomes progressively depleted in the eastonite component (by Tschermaks exchange).

Figure 8a shows a T–X_{H_2O} pseudosection at 3 kbar for the mean metapelite composition ($X_{Mg} = 0{\cdot}40$) that illustrates the influence of an H_2O-rich volatile phase (see White *et al.*, 2001). Such diagrams are useful for examining both subsolidus and suprasolidus evolution. The prograde subsolidus path will normally be buffered towards lower X_{H_2O}, as H_2O produced by dehydration reactions escapes into overlying (lower-T) rocks (Powell, 1983; Guiraud *et al.*, 2001). However, in the case of the Bushveld Complex aureole, this H_2O could have moved into hotter (suprasolidus) rocks and influenced melting behaviour (see Pattison & Harte, 1988).

Figure 8b shows an enlargement of part of Fig. 8a that illustrates the potential importance of H_2O-fluxed melting in the lower-grade migmatites. The white arrows show the possible prograde paths followed by the rocks, segments of which are discussed below.

Two paths are possible for the subsolidus evolution from ~630 to 640°C, both of which are predicted to produce prograde muscovite from a muscovite-absent assemblage, in apparent conflict with natural examples (see Pattison *et al.*, 2002). Path (i), in which H_2O is internally buffered, will result in volatile-phase consumption. Segment (ii) is possible if an external supply of H_2O is available. The modelled reaction associated with segment (ii) is

$$\mathrm{Bt + Sil + Qtz + H_2O \leftrightarrow (Pl) + Crd + Ms} \quad (4)$$

(phases in parentheses are minor reactants/products), which produces ~1·5 mol % muscovite.

The prograde evolution from ~640 to 650°C is characterized by a major dehydration step. The pulse of H_2O liberated along this segment potentially could have infiltrated overlying suprasolidus rocks. Segments (iii) and (iv) exhaust muscovite then sillimanite from the modelled bulk composition by the reactions

$$\begin{aligned}&\mathrm{(Pl) + (Crd) + Ms + Qtz}\\ &\mathrm{\leftrightarrow Kfs + (Bt) + Sil + H_2O}\end{aligned} \quad (5)$$

$$\mathrm{(Pl) + Bt + Sil + Qtz \leftrightarrow Kfs + Crd + H_2O.} \quad (6)$$

Reactions (5) and (6) liberate ~0·7 mol % H_2O. A minor amount (<0·1 mol %) of additional H_2O is liberated between 650 and 660°C along segment (v).

Upon reaching the solidus (black dot in Fig. 8a and b), prograde melt production is governed by both rising T and the supply of H_2O. A rise in T with no additional H_2O [segment (vi)] will result in the production of small quantities (<1 mol %) of melt, peritectic cordierite and K-feldspar, by reaction (3). For Fe-richer rocks that are Al-silicate bearing, reactions (2), and (2) and (1), will precede reaction (3) with decreasing X_{Mg} (<0·34 and <0·29, respectively), although the amount of melt produced will not be significantly higher (Fig. 7).

If at some fixed T along segment (vi) an influx of H_2O occurs [i.e. segment (vii)], the congruent reaction

$$\mathrm{Kfs + Pl + Bt + Crd + Qtz + H_2O \leftrightarrow L} \quad (7)$$

results in a five-fold increase in the melt fraction to 3·5–4·0 mol % for an addition of 0·7 mol % H_2O, the amount released by reactions (5) and (6). Melting by reaction (7) is not associated with any peritectic reaction products and leucosomes generated by the reaction will not include peritectic phases.

The pulse of H_2O supplied by reactions (5) and (6) occurs over a T interval of ~10°C. Consequently, in some of the overlying rocks, the prograde path is most likely to have followed a vector combining both rising T and additional H_2O. Segment (viii) shows the vector for a rock absorbing an ~0·7 mol % pulse of H_2O over ~10°C, the equivalent of absorbing the H_2O produced over the T interval of a prograde evolution along segments (iii) and (iv). Such a vector will be efficient at producing melt, as it is near orthogonal to the melt molar proportion isopleths, and will generate in excess of 4 mol % melt by reaction (7).

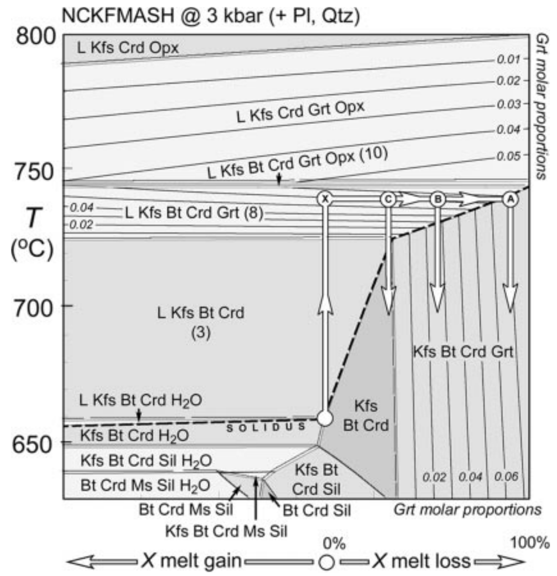

Fig. 9. T–X_{melt} pseudosection based on the mean metapelite composition. The garnet-bearing fields are contoured for molar proportions of garnet. The diagram considers an average regional metapelite heated to 740°C (up-T white arrow) at which point it contains ~12 mol % melt. A subsequent evolution to the right involves variable degrees (0–100%) of melt loss; to the left, the effect of melt gain is shown. The normalized bulk composition of the left- and right-hand edges of the diagram in terms of the components H_2O:SiO_2:Al_2O_3:CaO:MgO:FeO:K_2O:Na_2O are 14·91:70·22:6·98:0·19:0·27:1·20:3·62:2·61 and 2·92:63·77:14·39:0·60:6·34:9·19:1·86:0·93, respectively. Numbers in parentheses refer to the reaction (discussed in the text) that occurs across the relevant multivariant field. The darkest fields are quinivariant.

In reality, the prograde path may follow any vector with a positive slope in Fig. 8b, with the slope depending on the rates of T rise and H_2O supply. The rate of supply of H_2O to any particular volume of rock will be strongly influenced by the heterogeneity of volatile-phase distribution, i.e. whether transfer is pervasive or channelled. Vectors showing suprasolidus cordierite growth and/or consumption are shown in Fig. 8b. If the prograde vector is inclined more steeply ($> \mathrm{d}T/\mathrm{d}X_{H_2O}$) than the diagonal vector of constant cordierite molar proportion [e.g. along segment (ix)], peritectic cordierite is produced by an H_2O-fluxed variant of reaction (3). Pre-existing (mesosome) cordierite generated by subsolidus reaction is consumed by reaction (7) if the prograde vector is more shallow [e.g. along segment (viii)].

Higher-grade migmatites

For the mean metapelitic bulk composition ($X_{\mathrm{Mg}} = 0{\cdot}40$), between ~4 mol % (no H_2O influx) and ~9 mol % (0·7 mol % H_2O added) peritectic cordierite-bearing melt is predicted to have been produced by reaction (3) as T rose to ~725°C (Fig. 8a). Depending on the bulk-rock X_{Mg}, the first major melting step for most rocks ($X_{\mathrm{Mg}} < 0{\cdot}46$) occurs within the trivariant field {L + Kfs + Bt + Crd + Grt} by the volatile-phase-absent incongruent reaction

$$\mathrm{Pl + Bt + (Crd) + Qtz \leftrightarrow Kfs + Grt + L} \qquad (8)$$

marking the transition into the granulite facies in metapelites (Fig. 7). Proportions of cordierite remain effectively unchanged (i.e. mol % cordierite isopleths have a steep $\mathrm{d}T/\mathrm{d}X_{\mathrm{Mg}}$). The necessary aluminium for garnet is derived from biotite, which becomes progressively depleted in the eastonite component. Garnet-bearing leucosomes are common in metapelitic migmatite terrains and sillimanite-present variants of reaction (8) have been proposed to account for their formation (e.g. Grant, 1985*a*, 1985*b*; Le Breton & Thompson, 1988; Vielzeuf & Holloway, 1988; Waters, 1988; Powell & Downes, 1990; Carrington & Harley, 1995; Stevens *et al.*, 1997; Greenfield *et al.*, 1998; Johnson *et al.*, 2001*b*). Reaction (8) results in the production of up to 15 mol % additional melt over a restricted T range (<30°C), although the reaction is strongly dependent on X_{Mg} and is first encountered by Fe-richer rocks at ~690°C ($X_{\mathrm{Mg}} \sim 0{\cdot}25$), rising to ~745°C ($X_{\mathrm{Mg}} \sim 0{\cdot}46$; Fig. 7).

For the mean metapelite composition ($X_{\mathrm{Mg}} = 0{\cdot}40$), reaction (8) occurs at ~725°C; the T of reaction is essentially independent of whether H_2O is internally or externally buffered (Fig. 8a). Although the addition of H_2O will increase melt fractions (by ~5 mol % for ~1 mol % H_2O) by the congruent reaction

$$\mathrm{Kfs + Pl + (Bt) + (Crd) + (Grt)} \\ \mathrm{+ Qtz + H_2O \leftrightarrow L} \qquad (9)$$

this effect is proportionally small when compared with the effect of a similar H_2O influx at lower T. Melts produced by reaction (9) do not produce peritectic products and leucosomes will not include peritectic phases.

Figure 9 shows a T–X_{melt} diagram illustrating the effect of melt loss and melt gain (see White *et al.*, 2001; White & Powell, 2002) from the mean metapelitic bulk composition heated to 740°C (point X in Fig. 9). Reaction within the trivariant field {L + Kfs + Bt + Crd + Grt} [by reaction (8)] results in melt fractions increasing from ~4 to >12 mol % and the formation of ~6 mol % peritectic garnet, a quantity that is similar to that observed in the leucosome-deficient granofels. As melt is lost from the equilibration volume, the bulk composition will be displaced towards the right-hand edge of Fig. 9. If all of the melt is lost from the equilibration volume before significant cooling (point A), the rock will encounter the quadrivariant subsolidus field {Kfs + Pl + Bt + Crd + Grt + Qtz} with no resorption of garnet. The subvertical garnet molar proportion isopleths in this field (Fig. 9) indicate that subsequent cooling will have little or no effect on garnet content, particularly as diffusion will be greatly decreased in the absence of melt.

If some melt remains trapped within the equilibration volume, cooling results in garnet resorption, i.e. mol % garnet isopleths are subhorizontal within the melt-bearing field (Fig. 9). Point B shows a rock in which 60% of the 12 mol % melt is lost. The remaining 40% (~5 mol %) reacts with garnet on cooling by a reversal of reaction (8). As the last melt crystallizes, 2–3 mol % garnet remains. Garnet in such rocks would be expected to exhibit extensive reaction coronas (containing biotite and/or cordierite) and/or pronounced corrosion. If >60% melt remains (point C), complete garnet resorption is predicted on cooling (Fig. 9).

At ~750°C, orthopyroxene is expected as a peritectic product of melting in rocks with $X_{Mg} > 0{\cdot}35$ (Fig. 7). A significant quantity of melt (~5 mol %) is produced over a small T interval (~2°C) within the divariant field {Kfs + Bt + Crd + Grt + Opx} by the reaction

$$\begin{aligned} \mathrm{Pl + Bt + Grt + Qtz} &\leftrightarrow \\ \mathrm{Kfs + Crd + Opx + L} & \qquad (10) \end{aligned}$$

until either biotite or garnet is consumed (Fig. 7). In garnet-absent rocks ($X_{Mg} > 0{\cdot}46$) orthopyroxene and cordierite-bearing melts form (Fig. 7) by the reaction

$$\mathrm{Pl + Kfs + Bt + Qtz \leftrightarrow Crd + Opx + L.} \qquad (11)$$

Oxygen isotopes

Oxygen isotope analyses of whole-rock (WR) metapelite samples from the Silverton Formation were performed at Monash University on a Finnigan MAT 252 mass spectrometer. The method followed Clayton & Mayeda (1963), but using ClF_3 as the oxidizing reagent. Results are shown in Table 4 as $\delta^{18}O$ values expressed in per mil notation relative to V-SMOW. Internal standard BHQ was used for standardization, which has a long-term average $\delta^{18}O$ value of 10·24 ± 0·21‰ at Monash University. This standard was calibrated against NBS 28, which has a long-term average $\delta^{18}O$ value of 9·58 ± 0·12‰. Analysis of BHQ undertaken at the same time as analysis of the metapelitic rocks from the Silverton Formation averaged 10·33 ± 0·20‰ ($n = 16$).

The analysed rocks occur along strike over ~80 km from the 'Burgerfort Bulge' (Fig. 1) southwards as a function of decreasing contact metamorphic grade (latitude and longitude of samples are listed in Table 4). The lowest-grade rocks along the traverse are shales; at the highest grades the rocks are migmatites.

Table 4: Oxygen isotope data for Silverton Formation rocks

Sample	$\delta^{18}O_{WR}$	Lat. (S)	Long. (E)	Comment
2000BV-84	13·3	25°39·71′	30°14·57′	shale
2000BV-82	12·3	25°28·71′	30°21·69′	shale
2000BV-80	12·1	25°28·71′	30°21·69′	shale
2000BV-79	12·0	25°01·99′	30°25·45′	Mu–Chl
2000BV-78	11·7	25°01·99′	30°25·45′	Mu–Chl
2000BV-77	11·5	25°01·99′	30°25·45′	Mu–Chl
2000BV-74	12·1	24°56·15′	30°21·56′	Mu–Chl
2000BV-73	11·9	24°44·75′	30°22·84′	Crd–Bt
2000BV-72	11·9	24°44·75′	30°22·84′	Crd–Bt
2000BV-71	11·8	24°44·75′	30°22·84′	Crd–Bt
2000BV-68	12·2	24°44·75′	30°22·84′	Crd–Bt
2000BV-4	11·9	24°37·35′	30°21·07′	metatexite
2000BV-8	11·9	24°37·35′	30°21·07′	metatexite
2000BV-15	11·9	24°37·31′	30°21·03′	metatexite
2000BV-16	12·1	24°37·31′	30°21·03′	metatexite
2000BV-29	13·1	24°19·41′	30°02·68′	leucosome
2000BV-50	12·4	24°21·56′	29°42·57′	diatexite
2000BV-53	12·5	24°21·56′	29°42·57′	granite
2000BV-55	12·8	24°21·56′	29°42·57′	leucosome
2000BV-57	13·2	24°21·56′	29°42·57′	leucosome

Additionally, samples of decimetre- to metre-wide leucosomes and larger concordant peraluminous granite sheets were analysed from the core of the Zaaikloof fold structure, ~20 km to the NW of the Phepane fold in Fig. 1. Despite the range of metamorphic grades, there is little variation in $\delta^{18}O_{WR}$ values (11·5–13·3‰), and the maximum range occurs within low-grade samples. $\delta^{18}O_{WR}$ values are somewhat lower than expected based on compilations of oxygen isotope data from unmetamorphosed Phanerozoic shales ($\delta^{18}O_{WR}$ typically 14–19‰; Hoefs, 1997), but are within the range recorded from Proterozoic sediments (Schiffries & Rye, 1989).

Migmatitic metapelites that contain leucosomes too narrow to analyse separately show a very narrow range of $\delta^{18}O_{WR}$ values (11·9–12·4‰). Thicker, discrete leucosomes and larger granite sheets have $\delta^{18}O$ values (12·5–13·2‰) that are within the range typical of granites derived from the anatexis of sedimentary source rocks (Hoefs, 1997), and around 0·5–1‰ higher than those of the migmatitic host rocks. Given the mineralogy of the leucosomes, granite sheets and migmatitic metapelitic rocks, this difference is close to that expected from melts formed under closed-system conditions.

INTERPRETATION

Field and petrographic observations

Lower-grade migmatites

We suggest that metapelitic rocks in the aureole of the Bushveld Complex attained suffiently high T that they began to melt; at lower grades, metatexites were formed. Coarse discordant quartzofeldspathic leucosomes provide macroscopic evidence for the former presence of melt. At the thin-section scale, coarse quartzofeldpathic and muscovite-rich patches are present in quantities that are proportional to the degree of disruption of pre-migmatization structures, i.e. bedding. The coarse-grained nature of these leucocratic patches, their mineral assemblages [quartz, muscovite (probably after K-feldspar), plagioclase and fibrolite], their interstitial form, the low dihedral angles subtended with matrix phases (Laporte, 1994; Laporte *et al.*, 1997; Holness & Clemens, 1999) and the presence of euhedral, inclusion-free cordierite suggest that these leucocratic patches are pseudomorphs after melt pockets. We interpret euhedral cordierite within these patches as a prograde peritectic product of an incongruent biotite-consuming melting reaction.

The fibrolite seams are commonly associated with fibrolitized biotite and ilmenite (e.g. Fig. 4i and j). Such observations are consistent with base cation leaching of biotite by an acidic volatile phase (e.g. Wintsch, 1975; Vernon, 1979; Nabelek, 1997; McLelland *et al.*, 2002). The exsolution of ilmenite reflects the low solubility of Ti (and Fe) in the volatile phase. The general absence of K-feldspar from lower-grade rocks can be explained by metasomatism in the presence of a high a_{H+}/a_{K+} fluid (Nabelek, 1997). We interpret the fibrolite seams as pathways recording the passage of such an H_2O-rich volatile phase through the system. The seams splay at their margins into the mesosome (Fig. 2b), suggesting that the volatile phase was derived locally from the metapelitic rocks. The close association between fibrolite seams and the variably oriented foliation suggests that migration of the volatile phase was in part controlled by deformation, at least on a decimetre to metre scale.

Fibrolite and fibrolitized biotite are abundant within the stromatic quartz–sillimanite veins (Fig. 4i and j). We interpret the quartz–sillimanite veins as thin metapsammite or quartzite beds into which migration of volatiles was concentrated and implying a lithological control on fluid flow (see Watson, 1999). Thin melanosomes that border quartz–sillimanite veins suggest some volatile-fluxed reaction at the metapsammite–metapelite interface. Fluids (volatiles $\pm$ high a_{H_2O} melt) were preferentially channelled along the schistosity and through the quartz–sillimanite veins. Limited upward movement of the fluids occurred around ptygmatic folds where the foliation and fibrolite seams are steeply inclined.

At outcrop scale, steep fibrolite seams are closely associated with discordant leucosome (Figs 2d and 4l), suggesting that volatiles fluxed high a_{H_2O} melting. We infer that melt was unable to migrate any great distance from source. In thin section, fibrolite mats and seams that splay into leucocratic patches within mesosome usually terminate within a few millimetres or less (e.g. Fig. 4d), suggesting that migration of volatiles in these areas occurred on a similar scale. The retention of peritectic cordierite and its common alteration and hydration to pinite support the conclusion that melt movement was restricted and exsolved H_2O drove pinitization.

Matrix plagioclase commonly exhibits compositional zoning that is more strongly developed in fibrolite-rich rocks, where H_2O influx and melt fractions are inferred to have been greater. Such zoning profiles have been ascribed to disequilibrium reaction between crystallizing plagioclase and melt (e.g. Ashworth & McLennan, 1985).

Late tourmaline within highly disrupted, leucosome-rich rocks suggests that subsolidus matrix tourmaline contributed boron to flux melting (e.g. Pichavant, 1981), which then crystallized from melt on cooling. According to Spicer *et al.* (2002), boron-fluxed melting is unlikely to have a major effect on melt volumes. 'Late' muscovite, unrelated to fibrolite seams and leucocratic patches, overgrows the foliation and is interpreted to be the result of subsolidus rehydration, probably replacing K-feldspar.

Higher-grade migmatites

The higher-grade garnet granofels and inhomogeneous schollen diatexite preserve microstructures that strongly suggest the former presence of melt. Large euhedral garnets in the granofels have mantles rich in euhedral cordierite and rare subhedral zoned plagioclase that form a crystal-supported network (Fig. 5a), consistent with melt loss. Cuspate interstitial quartz patches (Fig. 5a) within the mantle represent the final sites of crystallization of melt trapped in pockets. An excess of SiO_2 evidently remained following diffusion of the other components of the crystallizing melt (i.e. K, Ca, Na, Al, $H_2O \pm$ Fe, Mg), which resulted in overgrowths on proximal matrix phases (dominantly plagioclase) and/or caused alteration and hydration of cordierite (to pinite), K-feldspar and/or albite (to white mica) and biotite (to chlorite).

Garnet also occurs within more continuous leucosome veins (Fig. 3a) that are interpreted to record macroscopic passage of melt through the granofels. Both garnet varieties are interpreted to be peritectic.

The strong spatial relationship between garnet and inferred sites of former melt implies co-nucleation of the solid and liquid products of the appropriate incongruent biotite-consuming, melting reaction (Powell & Downes, 1990).

The inhomogeneous diatexite is interpreted to represent the product of net melt accumulation, a conclusion supported by the high modal abundance of leucosome and the leucosome-supported microstructures (Fig. 5c and d). The hydrous nature of the matrix assemblage (i.e. muscovite, pinitized cordierite) is interpreted to reflect reaction between the matrix and peritectic phases with crystallizing melt as it exsolved H_2O. Much of the melt inferred to have been present in these rocks may have been derived following melt–residuum separation and flow of material away from the granofels, a process that is diagnostic of diatexite formation (e.g. Brown, 1973; Sawyer, 1996).

The leucodiatexite hosting the norite fragments at the RLS contact has a mineral assemblage and microstructure typical of granite, suggesting that it is predominantly composed of crystallized melt. The pronounced biotite-rich rims around norite xenoliths (Fig. 3c and d) suggest reaction with melt. The abundance of frozen melt and the general lack of ferromagnesian peritectic phases that would be expected if the melt was produced from *in situ* melting of the metapelitic rocks suggests that the melt was derived by efficient melt–residuum unmixing of an underlying fertile source. We interpret the abundant rounded quartz grains to imply disaggregation of host Lakenvalei Formation quartzite as ascending melts moved into and through the system.

Phase equilibria and anatexis

Lower-grade migmatites

The presence or absence of andalusite in metapelitic rocks at lower grade can be explained by the variation in X_{Mg} of the protolith (Fig. 7). High-T subsolidus reaction in quartz-present metapelitic rocks is characterized by dehydration of muscovite [reaction (5)] followed by biotite + sillimanite [reaction (6)], which results in the production of ~0·7 mol % H_2O over ~10°C. We suggest that the liberated H_2O interacted with overlying, suprasolidus rocks and variably fluxed melting. Suprasolidus volatile-phase-absent reactions for all metapelitic rocks at lower grade ($T < 690$°C) produce small volumes of high-a_{H_2O} peritectic cordierite-bearing melt by reactions (1), (2) and/or (3) (Fig. 7). With an influx of H_2O, cordierite-bearing melts are also produced by an H_2O-fluxed variant of reaction (3), provided the dT/X_{H_2O} of the prograde vector is steeper than constant cordierite mol % isopleths (>10°C/0·7 mol % H_2O; Fig. 8b).

Evidence for these reactions is preserved within both andalusite-bearing and andalusite-free Silverton Formation metatexites. Small, coarse-grained leucocratic patches that are interpreted to represent pseudomorphs after pockets of high-a_{H_2O} melt are ubiquitously associated with euhedral peritectic cordierite. Corroded reactant andalusite poikiloblasts associated with these patches controlled sites of melt nucleation by reactions (1) and/or (2) in Fe-richer rocks (Fig. 4d and e). Within more magnesian, andalusite-free rocks, these patches (Fig. 4f and g) are more widely dispersed throughout the rock volume, reflecting a more homogeneous distribution of reactant matrix phases (principally biotite) involved in reaction (3).

With greater H_2O influx (shallow dT/X_{H_2O}; Fig. 8b), cordierite consumption is predicted and larger volumes (~4 mol %) of high-a_{H_2O} melts will be produced by the congruent reaction (7) (Fig. 8b). Such melts will not be associated with any peritectic phases. In the metatexites, the overall abundance of discontinuous leucosomes, their coarse-grained nature and the common (but not ubiquitous) absence of peritectic cordierite are consistent with their derivation by melting driven by an influx of a larger volume of H_2O vapour. The steeply inclined fibrolite seams that are commonly associated with discordant leucosomes (Fig. 4d and e) are interpreted to have been the major conduits through which H_2O from underlying, dehydrating rocks was channelled upwards to flux melting. Subhorizontal volatile-phase flow along stromatic quartz–sillimanite veins that fed the steeply inclined fibrolite seams also caused H_2O-fluxed melting at the vein–mesosome interface [by reaction (7)], forming residual biotite-rich melanosomes.

Higher-grade migmatites

The coarse-grained, leucosome-poor granofels on the margins of the Steelpoort dome contains abundant peritectic cordierite and garnet, consistent with the higher T predicted here (~725°C; Fig. 6) and the operation of the volatile-phase-absent reaction (8). Cordierite is not a product of this reaction and its abundance in the higher-grade rocks is interpreted to have been the result of lower-T prograde melting. The modal abundance of cordierite, which may comprise $\gg$50 vol. %, biotite and garnet and the scarcity of quartz imply residual bulk compositions (Mg, Fe and Al rich, Si poor) and loss of melt.

Although a limited degree of retrogression is evident in thin section, the granofels contains garnets with perfect crystal faces and exhibits texturally equilibrated microstructures that suggest retrogression was minimal. X-ray composition maps show that garnets of all sizes are unzoned, apart from at their extreme edges, consistent with this conclusion. If a significant amount of melt remained trapped within the equilibration volume, garnet should have been strongly resorbed (Fig. 9). The evidence suggests that the modal quantities of garnet present in the Vermont Formation granofels approximates that predicted at the metamorphic peak (~6 mol %) and that >90% of the melt produced was removed. Microstructures (Figs. 5b) and the scarcity of leucosome in these rocks attest to the efficacy of this process.

The inhomogeneous diatexite is garnet free and contains abundant coarse biotite. Euhedral pinitized cordierite and zoned plagioclase are surrounded by large patches of muscovite, quartz and plagioclase (Fig. 5c and d) that are interpreted to represent frozen melt. The leucosome-rich and former melt-supported nature of these rocks and the hydrous nature of the matrix assemblage suggest that the melt fraction was large and that much of the melt was retained. The inhomogeneous diatexite probably represents a site of net melt accumulation (i.e. the bulk composition plots to the right of point X in Fig. 9), possibly following flow of melt out of the neighbouring granofels.

At the T predicted at the contact, orthopyroxene is expected as a peritectic product of melting. Orthopyroxene with both garnet and cordierite is reported from residual metapelitic rocks at and within the RLS contact (Willemse & Viljoen, 1970; Engelbrecht, 1990). Mass-balance considerations suggest that these rocks lost up to 65 vol. % granitic melt locally (Nell, 1985).

Limitations of the model

A limitation to the NCKFMASH model system in modelling phase relations in the Bushveld migmatites is the general absence of K-feldspar from all rocks other than the homogeneous leucodiatexite. K-feldspar is predicted as a product of high-T subsolidus dehydration and suprasolidus melting equilibria in the model system, and should be a product of crystallizing melt. Its absence may be due to one or a combination of: (1) retrograde reaction of K-feldspar with melt and/or an H_2O-rich volatile phase to form muscovite (e.g. Kohn *et al.*, 1997); (2) preferential leaching of K-feldspar by an acidic volatile phase (e.g. Nabelek, 1997); (3) the presence of additional components, principally Ti and Fe^{3+} (O_2), which will increase biotite stability relative to K-feldspar; (4) an overestimation of H_2O contents (and H_2O/K_2O ratios) in the thermodynamic melt model (Carrington & Watt, 1995); (5) loss of the melt phase. It is difficult to quantify the relative importance of these processes. However, there is good evidence for the presence of high-a_{H^+}/a_{K^+} fluids in lower-grade rocks; coarse intergrowths of muscovite + quartz and plagioclase + quartz myrmekites in leucosome-rich portions of all migmatites indicate some retrograde reaction of K-feldspar with crystallizing melt.

Oxygen isotopes and aureole-scale migration of volatiles

In contact aureoles with subhorizontal sedimentary layering that includes impermeable units such as quartzites and marbles, as in the floor of the Bushveld Complex, large-scale migration of volatiles in metapelitic units is likely to be layer-parallel. In the study area, magmatic rocks of the RLS cut down through the floor rocks in the 'Burgersfort Bulge' (Fig. 1). Therefore layer-parallel volatile-phase flow should occur along thermal gradients either towards (up-T flow of volatiles derived from dehydration of the aureole rocks) or away from (down-T flow of a magma-derived volatile phase) the 'Burgersfort Bulge'. Up- and down-T flow of volatiles potentially should cause different patterns of isotopic resetting (Dipple & Ferry, 1992).

The oxygen isotope data from the Silverton Formation metapelitic rocks (Table 4) place further constraints on the relationship between volatile-phase flow and melting in the aureole. In the absence of any large-scale migration of volatiles, closed-system devolatilization alone will reduce $\delta^{18}O$ values by up to 1‰ (Chamberlain *et al.*, 1990), which could account for the maximum observed $\delta^{18}O$ variation in the Silverton Formation rocks as a function of grade. The data explicitly preclude the possibility that partial melting was fluxed by volatiles exsolved from, or equilibrated with, the magmatic rocks of the RLS. In particular, given the average $\delta^{18}O_{Opx}$ value in the RLS rocks (6·7‰; Schiffries & Rye, 1989), the expected $\Delta^{18}O_{Opx\text{-}H_2O}$ (−1·88‰ at 700°C; Zheng, 1993), and that K-feldspar can be used as a proxy for $\delta^{18}O_{WR}$ in metapelitic or quartzofeldspathic rocks (Friedman & O'Neil, 1977, fig. 25; Cartwright *et al.*, 1996), metapelitic rocks in O-isotope equilibrium with a fluid derived from, or equilibrated with, the RLS at T applicable to migmatization of the Silverton Formation would have had a $\delta^{18}O_{WR}$ of ~8·70‰ ($\Delta^{18}O_{K\text{-feldspar-}H_2O}$ = 0·12‰ at 700°C; Zheng, 1993). Migmatitic Silverton Formation metapelitic rocks and macroscopic leucosomes and granite sheets have considerably higher $\delta^{18}O_{WR}$ values that are essentially identical to the lower-grade, unmelted Silverton Formation metapelitic rocks (Table 4). This suggests that down-T flow of a magmatic volatile phase did not drive H_2O-fluxed partial melting in the lower-T portion of the migmatitic zone.

Aureole-scale up-T flow of volatiles derived from dehydration of the lower-grade Silverton Formation metapelitic rocks should result in smooth profiles of decreasing $\delta^{18}O_{WR}$ with increasing metamorphic grade unless time-integrated volatile fluxes were small, in which case little or no isotopic resetting would occur (Dipple & Ferry, 1992). The lack of oxygen isotope resetting as a function of increasing metamorphic grade is therefore consistent with either no aureole-scale flow of volatiles, or minor up-T flow; enough to locally flux partial melting but not enough to lower $\delta^{18}O_{WR}$ values. This is consistent with petrological evidence.

DISCUSSION

Metamorphism and anatexis

During prograde regional metamorphism, hydrous minerals break down to produce a free volatile phase that we assume will normally escape into overlying, cooler rocks. In mica-rich metaclastic sequences, the supercritical volatile phase will dominantly comprise H_2O with variable quantities of dissolved species that may result in quartz ($\pm$feldspar) vein precipitation at shallower crustal levels. Upon reaching the solidus, the volatile phase becomes metastable with respect to melt and mica breakdown produces small quantities of granitic liquid. Higher T results in an increased quantity of H_2O-undersaturated, hydroscopic melt and the supply of H_2O to overlying rocks stops. In such circumstances, and in the absence of an exotic, externally derived volatile influx, major melt generation in metapelitic rocks will occur only when T is sufficiently high for volatile-phase-absent reaction. Such reactions lead to rapid, step-like production of low-a_{H_2O} melts within low-variance fields (e.g. Vielzeuf & Holloway, 1988).

In the Bushveld Complex, extreme contact metamorphic T was superimposed upon a regional geotherm to produce a transient inverted thermal gradient in the aureole rocks beneath the RLS. As particular rocks reached the solidus, underlying cooler rocks were dehydrating, thus providing a source of upward-migrating H_2O to flux melting in hotter, shallower rocks. Although the metastable presence of andalusite attests to a degree of disequilibrium within the migmatites, the inferred presence of melt as a diffusion-enhancing medium suggests that equilibrium conditions could have been approached in the inner aureole. In general, the mineral chemistry and microstructures support an assumption of textural and chemical equilibrium. Accepting the limitations inherent in the model system, particularly the lack of K-feldspar in the rocks, calculated equilibrium phase relations in the NCKFMASH model system compare favourably with the observed parageneses and allow a semi-quantitative interpretation of the prograde and retrograde evolution of the rocks.

Immediately after intrusion of the RLS, contact rocks of suitable composition began to melt. As the intrusion cooled, the underlying rocks continued to heat; the metamorphic peak was reached successively later with increasing depth. Rocks within $\sim$100 m of the contact reached their thermal peak within $\sim$75 kyr after intrusion and attained sufficiently high T for volatile-phase-absent, biotite-consuming melting to occur. Such reactions produce strongly H_2O-undersaturated melts with ferromagnesian peritectic by-products and are characterized by molar melt proportion isopleths that have a positive dP/dT. Such conditions favour melt ascent (e.g. Clemens & Droop, 1998). The inverted thermal gradient beneath the Bushveld Complex and the consequent decrease in melt viscosity on ascent would have further aided upward melt migration.

Rocks between $\sim$100 and 750 m from the contact melted but did not attain sufficiently high T for major melt production via volatile-phase-absent reaction. During the melting interval, metatexites were supplied with H_2O from surrounding and underlying, dehydrating rocks. Local (millimetre-scale) redistribution of H_2O fluxed biotite-consuming incongruent melting in mesosomes, and resulted in the production of low-volume peritectic cordierite-bearing melt pockets. Larger volumes of structurally focused volatile-phase influx resulted in congruent melting and the production of larger melt volumes, preserved as discordant leucosome. These high-a_{H_2O} melts were unable to migrate significant distances from their source (Clemens & Droop, 1998).

Fluid flow

Oxygen isotope measurements suggest that little or no aureole-scale flow of volatiles occurred and that, consequently, the H_2O inferred to have fluxed melting was locally redistributed (i.e. on an outcrop scale). Metapelitic rocks cannot have interacted with magmatic fluids derived from the RLS, precluding large-scale pluton-driven convection that may generate a variety of flow patterns in contact aureoles (e.g. Hanson, 1992).

At lower grades, fibrolite mats and seams are interpreted to record decimetre- to metre-scale volatile-phase flow. The close association between fibrolite seams, stromatic quartz–sillimanite veins, the variably inclined foliation and discordant leucosome suggests a genetic relationship between volatile-phase influx, melting and deformation. Within the mesosome, the schistosity and fibrolite seams are most commonly at a low angle to bedding. We interpret the driving force for subhorizontal flow of volatiles to have been compaction associated with the weight of the overlying RLS. The volatile phase was preferentially channelled from metapelite into thin metapsammite horizons that are represented by the quartz–sillimanite veins, causing congruent melting at the vein–mesosome interface.

Subsequent upward fluid migration (volatiles ± high-a_{H_2O} melt) occurred locally along a steep schistosity that developed in response to ptygmatic fold formation. Small-scale folds were probably parasitic to the regional periclinal folds (Fig. 1), which have been interpreted as resulting from diapiric rise of floor rocks into the base of the RLS (Uken & Watkeys, 1997). Volatile flux through and/or into structurally controlled sites (e.g. Fig. 2a, c and d) promoted congruent melting and discordant leucosome formation.

At higher grades, where melt fractions were larger, small-scale structures are not present. However, the granofels, inhomogeneous diatexite and homogeneous leucodiatexite occur within the core of regional-scale anticlinal periclinal folds (at Steelpoort and Derde Gelid, respectively; Fig. 1). We suggest there may be a genetic relationship between megascopic dome formation and upward migration of low a_{H_2O} melt. It is possible that the periclines were the focus for diapiric rise of melt into the basal portions of the ultramafic RLS rocks. Such magma–country rock interactions may have important implications for the isotopic and mineralogical evolution of the RLS (e.g. Cawthorn *et al.*, 1985).

CONCLUSIONS

Migmatites in metapelitic rocks in the aureole beneath the Bushveld Complex preserve evidence for low- and high-a_{H_2O} melting. Leucocratic patches and macroscopic discordant leucosomes within lower-grade metatexites represent sites of melt crystallization. Thin fibrolite seams are interpreted to record passage of high-a_{H^+}/a_{K^+} volatiles through the system. Millimetre-scale quartzofeldspathic and muscovite-rich patches represent pseudomorphs after pockets of melt produced by incongruent breakdown of biotite. Melting was potentially fluxed by small volumes of locally derived H_2O. Coarse-grained discordant leucosomes have similar compositions to the patches but form segregations that are two orders of magnitude larger. The discordant nature of these bodies and their ubiquitous association with fibrolite seams imply greater melt production. These larger melt volumes are interpreted to have resulted from congruent melting that was fluxed by a structurally controlled infiltration of an H_2O-rich volatile phase derived from underlying (cooler) dehydrating rocks. Melts at lower grade were essentially immobile.

At higher structural levels, temperatures were sufficiently high for the generation of larger volumes of melt (>10 mol %) by volatile-phase-absent, biotite-consuming incongruent reactions that produced peritectic garnet, cordierite and/or orthopyroxene. H_2O from underlying rocks may have contributed to the formation of cordierite-bearing melts early in the suprasolidus history, increasing melt fractions. At elevated T, however, such a supply is highly unlikely given that underlying rocks were partially molten and would consequently have acted as an H_2O sink. The residual composition and the microstructures preserved within the garnet granofels imply extreme melt loss and efficient solid–melt unmixing. The higher predicted melt fractions are interpreted to have enabled deformation-driven flow of melt away from the solid residue (Sawyer, 1996; Rutter, 1997). Small, irregular leucosome veins are interpreted to record passage of melt through the compacting granofels matrix. Although some of the fugitive melt was retained in neighbouring heterogeneous diatexite, it is likely that much escaped to higher levels.

At the contact, fragments of brecciated RLS marginal zone norite lie within homogeneous leucodiatexite that has a typical granitic composition and microstructure and is interpreted to largely represent frozen melt. The norite xenoliths have pronounced reaction rims dominated by biotite, suggesting reaction with melt. The leucodiatexite is almost completely devoid of mafic peritectic and retrogressive phases. The large volumes of melt present are interpreted to have been derived from deeper levels. Residual granulite-facies granofels similar to those described from the Steelpoort area may have been the source for leucodiatexite at the contact.

ACKNOWLEDGEMENTS

We thank Phil Piccoli for help with EPMA data collection and interpretation. Jeanne Martin's tabulating skills are gratefully acknowledged. We appreciate field guidance and discussion with Johann Kruger and the hammer skills of Elke Graf. Peter Nabelek, Dave Pattison and Harold Stowell are thanked for detailed and perceptive reviews. Any errors and/or misinterpretations are ours. We thank George Bergantz for his encouragement and expeditious editorial handling. T.E.J. and M.B. acknowledge financial support from the University of Maryland. R.L.G. acknowledges financial support from the University of the Witwatersrand; I.S.B. acknowledges an ARC Senior Research Fellowship and an IREX grant.

REFERENCES

Ashworth, J. R. & McLennan, E. L. (1985). Textures. In: Ashworth, J. R. (ed.) *Migmatites*. Glasgow: Blackie, pp. 180–203.

Brown, M. (1973). The definition of metatexis, diatexis and migmatites. *Proceedings of the Geologists' Association* **84**, 371–382.

Brown, M. (1994). The generation, segregation, ascent and emplacement of granite magma: the migmatite-to-crustally-derived granite connection in thickened orogens. *Earth-Science Reviews* **36**, 83–130.

Brown, M. & Solar, G. S. (1999). The mechanism of ascent and emplacement of granite magma during transpression: a syntectonic granite paradigm. *Tectonophysics* **312**, 1–33.

Brown, M., Averkin, Y. A., McLellan, E. L. & Sawyer, E. W. (1995). Melt segregation in migmatites. *Journal of Geophysical Research* **100**, 15655–15679.

Buick, I. S., Maas, R. & Gibson R. (2001). Precise U–Pb titanite age constraints on the emplacement of the Bushveld Complex, South Africa. *Journal of the Geological Society, London* **158**, 3–6.

Bumby, A. J., Eriksson, P. G. & Van der Merwe, R. (1998). Compressive deformation in the floor rocks to the Bushveld Complex (South Africa): evidence from the Rustenburg Fault Zone. *Journal of African Earth Sciences* **27**, 307–330.

Button, A. (1978). Diapiric structures in the Bushveld, north-eastern Transvaal. *Economic Geology Research Unit, University of the Witwatersrand Information Circular* **96**, 13.

Carrington, D. P. & Harley, S. L. (1995). Partial melting and phase relations in high-grade metapelites: an experimental petrogenetic grid in the KFMASH system. *Contributions to Mineralogy and Petrology* **120**, 270–291.

Carrington, D. P. & Watt, G. R. (1995). A geochemical and experimental study of the role of K-feldspar during water-undersaturated melting of metapelites. *Chemical Geology* **122**, 59–76.

Cartwright, I., Buick, I. S. & Vry, J. K. (1996). Polyphase metamorphic fluid flow in the Lower Calcsilicate Unit, Reynolds Range, central Australia. *Precambrian Research* **77,** 211–229.

Cawthorn, R. G. & Walraven, F. (1998). Emplacement and crystallization time for the Bushveld Complex. *Journal of Petrology* **39**, 1669–1687.

Cawthorn, R. G., Barton, J. M., Jr & Viljoen, M. J. (1985). Interaction of floor rocks with the Platreef on Overysel, Potgietersrus, northern Transvaal. *Economic Geology* **80**, 988–1006.

Chamberlain, C. P., Ferry, J. M. & Rumble, D. I. (1990). The effect of net-transfer reactions on the isotopic composition of minerals. *Contributions to Mineralogy and Petrology* **105**, 322–336.

Clayton, R. N. & Mayeda, T. K. (1963). The use of bromine pentafluoride in the extraction of oxygen from oxides and silicates for isotopic analyses. *Geochimica et Cosmochimica Acta* **27**, 43–52.

Clemens, J. D. & Droop, G. T. R. (1998). Fluids, P–T paths and the fates of anatectic melts in the Earth's crust. *Lithos* **44**, 21–36.

Connolly, J. A. D. & Thompson, A. B. (1989). Fluid and enthalpy production during regional metamorphism. *Contributions to Mineralogy and Petrology* **102**, 347–366.

De Waal, S. A. (1970). Interference folding of Bushveld Igneous Complex age in the Transvaal Sequence north of Marble Hall. In: Visser, D. J. L. & von Gruenewaldt, G. (eds) *Symposium on the Bushveld and other Layered Intrusives. Geological Society of South Africa, Special Publications* **1**, 283–298.

Dipple, G. M. & Ferry, J. M. (1992). Fluid flow and stable isotopic alteration in rocks at elevated temperatures with applications to metamorphism. *Geochimica et Cosmochimica Acta* **56**, 3539–3550.

D'Lemos, R. S., Brown, M. & Strachan, R. A. (1992). Granite magma generation, ascent and emplacement within a transpressional orogen. *Journal of the Geological Society, London* **149**, 487–490.

Droop, G. T. R., Clemens, J. D. & Dalrymple, D. J. (2003). Contact anatexis of metapelites, melt escape and restite formation in the Huntly Gabbro Complex, NE Scotland: an integrated investigation. *Journal of Petrology* **44** (in press).

Ebadi, A. & Johannes, W. (1991). Beginning of melting and composition of first melts in the system Qz–Ab–Or–H_2O–CO_2. *Contributions to Mineralogy and Petrology* **106**, 286–295.

Engelbrecht, J. P. (1990). Contact metamorphic processes related to the aureole of the Bushveld Complex in the Marico District, western Transvaal, South Africa. *South African Journal of Geology* **93**, 339–349.

Friedman, I. & O'Neil, J. R. (1977). Compilation of stable isotope fractionation factors of geochemical interest. In: Fleischer, M. (ed.) *Data of Geochemistry. US Geological Survey Professional Paper* **440-KK**.

Grant, J. A. (1985*a*). Phase equilibria in low-pressure partial melting of pelitic rocks. *American Journal of Science* **285**, 409–435.

Grant, J. A. (1985*b*). Phase equilibria in partial melting of pelitic rocks. In: Ashworth, J. R. (ed.) *Migmatites*. Glasgow: Blackie, pp. 86–144.

Greenfield, J. E., Clarke, G. L. & White, W. (1998). A sequence of partial melting reactions at Mount Stafford, central Australia. *Journal of Metamorphic Geology* **16**, 363–378.

Guiraud, M., Powell, R. & Rebay, G. (2001). H_2O in metamorphism and unexpected behaviour in the preservation of metamorphic mineral assemblages. *Journal of Metamorphic Geology* **19**, 445–454.

Hanson, R. B. (1992). Effects of fluid production on fluid flow during regional and contact metamorphism. *Journal of Metamorphic Geology* **10**, 87–97.

Hartel, T. H. D. & Pattison, D. R. M. (1996). Genesis of the Kapuskasing (Ontario) migmatitic mafic granulites by dehydration melting of amphibolite: the importance of quartz to reaction progress. *Journal of Metamorphic Geology* **14**, 591–611.

Hartzer, F. J. (1995). Transvaal Supergroup inliers: geology, tectonic development and relationship with the Bushveld Complex, South Africa. *Journal of African Earth Sciences* **21**, 521–547.

Hiemstra, S. A. & van Biljon, W. J. (1959). The geology of the Upper Magaliesburg Stage and the Lower Bushveld Complex in the vicinity of Steelpoort. *Transactions of the Geological Society of South Africa* **62**, 239–255.

Hoefs, J. (1997). *Stable Isotope Geochemistry*. Berlin: Springer.

Holland, T. J. B. & Powell, R. (1998). An internally consistent thermodynamic data set for phases of petrological interest. *Journal of Metamorphic Geology* **16**, 309–343.

Holland, T. J. B. & Powell, R. (2001). Calculation of phase relations involving haplogranite melts using an internally consistent dataset. *Journal of Petrology* **42**, 673–683.

Holness, M. B. & Clemens, J. D. (1999). Partial melting of the Appin Quartzite driven by fracture-controlled H_2O infiltration in the aureole of the Ballachulish Igneous Complex, Scottish Highlands. *Contributions to Mineralogy and Petrology* **136**, 154–168.

Johannes, W. (1984). Beginning of melting in the granite system Qz–Or–Ab–An–H_2O. *Contributions to Mineralogy and Petrology* **86**, 264–273.

Johnson, T. E., Hudson, N. F. C. & Droop, G. T. R. (2001*a*). Melt segregation structures within the Inzie Head gneisses of the northeastern Dalradian. *Scottish Journal of Geology* **37**, 59–72.

Johnson, T. E., Hudson, N. F. C. & Droop, G. T. R. (2001*b*). Partial-melting in the Inzie-Head gneisses: the role of water and a petrogenetic grid in KFMASH applicable to anatectic pelitic migmatites. *Journal of Metamorphic Geology* **19**, 99–118.

Kalt, A., Altherr, R. & Ludwig, T. (1998). Contact metamorphism in politic rocks on the Island of Kos (Greece, eastern Aegean Sea): a test for the Na-in-cordierite thermometer. *Journal of Petrology* **39**, 663–688.

Kohn, M. J., Spear, F. S. & Valley, J. W. (1997). Dehydration-melting and fluid recycling during metamorphism: Rangeley Formation, New Hampshire, USA. *Journal of Petrology* **38**, 1255–1277.

Kretz, R. (1983). Symbols for rock forming minerals. *American Mineralogist* **68**, 277–279.

Laporte, D. (1994). Wetting behaviour of partial melts during crustal anatexis: the distribution of hydrous silicic melts in polycrystalline aggregates of quartz. *Contributions to Mineralogy and Petrology* **116**, 486–499.

Laporte, D., Rapaille, C. & Provost, A. (1997). Wetting angles, equilibrium melt geometry, and the permeability threshold of partially molten crustal protoliths. In: Bouchez, J. L., Hutton, D. W. H. & Stephens, W. E. (eds) *Granite: from Segregation of Melt to Emplacement Fabrics*. Dordrecht: Kluwer Academic, pp. 31–54.

Le Breton, N. & Thompson, A. B. (1988). Fluid-absent (dehydration) melting of biotite in metapelites in the early stages of crustal anatexis. *Contributions to Mineralogy and Petrology* **99**, 226–237.

Marchildon, N. & Brown, M. (2002). Grain-scale melt distribution in two contact aureole rocks: implications for controls on melt localization and deformation. *Journal of Metamorphic Geology* **20**, 381–396.

McLelland, J., Morrison, J., Selleck, B., Cunningham, B. Olson, C. & Schmidt, K. (2002). Hydrothermal alteration of late- to post-tectonic Lyon Mountain Granitic Gneiss, Adirondack Mountains, New York: origin of quartz–sillimanite segregations, quartz–albite lithologies, and associated Kiruna-type low-Ti Fe-oxide deposits. *Journal of Metamorphic Geology* **20**, 175–190.

Mehnert, K. R. (1968). *Migmatites and the Origin of Granitic Rocks*. Amsterdam: Elsevier.

Mirwald, P. W. (1986). Ist Cordierit ein Geothermometer. *Fortschritte der Mineralogie* **64**, 119.

Nabelek, P. I. (1997). Quartz–sillimanite leucosomes in high-grade schists, Black Hills, South Dakota: a perspective on the mobility of Al in high-grade metamorphic rocks. *Geology* **25**, 995–998.

Nell, J. (1985). The Bushveld metamorphic aureole in the Potgietersrus area: evidence for a two-stage metamorphic event. *Economic Geology* **80**, 1129–1152.

Nelson, D. R., Trendall, A. F. & Altermann, W. (1999). Chronological correlations between Pilbara and Kaapvaal cratons. *Precambrian Research* **97**, 165–189.

Pattison, D. R. M. & Harte, B. (1988). Evolution of structurally contrasting anatectic migmatites in the 3-kbar Ballachulish aureole, Scotland. *Journal of Metamorphic Geology* **6**, 475–494.

Pattison, D. R. M., Spear, F. S., Debuhr, C. L., Cheney, J. T. & Guidotti, C. V. (2002). Thermodynamic modeling of the reaction muscovite + cordierite $\rightarrow Al_2SiO_5$ + biotite + quartz + H_2O: constraints from natural assemblages and implications for the metapelitic petrogenetic grid. *Journal of Metamorphic Geology* **20**, 99–118.

Pichavant, M. (1981). An experimental study of the effect of boron on a water-saturated haplogranite at 1 kbar pressure. Geological applications. *Contributions to Mineralogy and Petrology* **76**, 430–439.

Powell, R. (1983). Fluids and melting under upper amphibolite facies conditions. *Journal of the Geological Society, London* **140**, 629–633.

Powell, R. & Downes, J. (1990). Garnet porphyroblast-bearing leucosomes in metapelites: mechanisms, phase diagrams, and an example from Broken Hill, Australia. In: Ashworth, J. R. & Brown, M. (eds) *High-Temperature Metamorphism and Crustal Anatexis*. London: Unwin, pp. 105–123.

Powell, R. & Holland, T. J. B. (1988). An internally consistent thermodynamic dataset with uncertainties and correlations. III. Application methods, worked examples and a computer program. *Journal of Metamorphic Geology* **6**, 173–204.

Rutter, E. H. (1997). The influence of deformation on the extraction of crustal melts: a consideration of the role of melt-assisted granular flow. In: Holness, M. (ed.) *Deformation-Enhanced Melt Segregation and Metamorphic Fluid Transport. Mineralogical Society Series 8*. London: Chapman and Hall, pp. 82–110.

Sawyer, E. W. (1994). Melt segregation in the continental crust. *Geology* **22**, 1019–1022.

Sawyer, E. W. (1996). Melt-segregation and magma flow in migmatites: implications for the generation of granitic magmas. *Transactions of the Royal Society of Edinburgh: Earth Sciences* **87**, 85–94.

Sawyer, E. W. (2001). Melt segregation in the continental crust: distribution and movement of melt in anatectic rocks. *Journal of Metamorphic Geology* **19**, 291–309.

Schiffries, C. M. & Rye, D. M. (1989). Stable isotopic systematics of the Bushveld Complex: I. Constraints of magmatic processes in layered intrusions. *American Journal of Science* **289**, 841–873.

Sharpe, M. R. & Chadwick, B. (1982). Structures in Transvaal sequence rocks within and adjacent to the Eastern Bushveld Complex. *Transactions of the Geological Society of South Africa* **85**, 29–41.

Sharpe, M. R. & Hulbert, L. J. (1985). Ultramafic sills beneath the Eastern Bushveld Complex: mobilized suspensions of early Lower Zone cumulates in a parental magma with boninitic affinities. *Economic Geology* **80**, 849–871.

Spicer, E., Stevens, G., Buick, I. S. & Terlet, J (2002). Experimental constraints on the role of boron in the low-pressure fluid-absent partial melting of metapelites from the Mount Stafford area, central Australia. In: Preiss, V. P. (ed.) *Geoscience 2002: Expanding Horizons. Abstracts of the 16th Australian Geological Convention, Adelaide Convention Centre, Adelaide, S.A.*, **67**, 217.

Stevens, G., Clemens, J. D. & Droop, G. T. R. (1997). Melt production during granulite-facies anatexis: experimental data from 'primitive' metasedimentary protoliths. *Contributions to Mineralogy and Petrology* **128**, 352–370.

Tinkham, D. K., Zuluaga, C. A. & Stowell, H. H. (2001). Metapelitic phase equilibria modelling in MnNCKFMASH: the effect of variable Al_2O_3 and MgO/(MgO + FeO) on mineral stability. *Geological Materials Research* **3**, 1–42.

Uken, R. & Watkeys, M. K. (1997). Diapirism initiated by the Bushveld Complex, South Africa. *Geology* **25**, 723–726.

Vernon, R. H. (1979). Formation of late sillimanite by hydrogen metasomatism (base-leaching) in some high-grade gneisses. *Lithos* **12**, 143–152.

Vielzeuf, D. & Hollaway, J. R. (1988). Experimental determination of the fluid-absent melting reactions in the pelite system. *Contributions to Mineralogy and Petrology* **98**, 257–276.

Walraven, F. (1997). Geochronology of the Rooiberg Group, Transvaal Supergroup, South Africa. *Information Circular, Economic Geology Research Unit, University of the Witwatersrand* **316**.

Walraven, F., Armstrong, R. A. & Kruger, F. J. (1990). A chronostratigraphic framework for the north-central Kaapvaal Craton, the Bushveld Complex and Vredefort structure. *Tectonophysics* **171**, 23–48.

Waters, D. J. (1988). Partial melting and the formation of granulite facies assemblages in Namaqualand, South Africa. *Journal of Metamorphic Geology* **6**, 387–404.

Waters, D. J. & Lovegrove, D. P. (2002). Assessing the extent of disequilibrium and overstepping of prograde metamorphic reactions in metapelites from the Bushveld aureole. *Journal of Metamorphic Geology* **20**, 135–149.

Watson, E. B. (1999). Lithologic partitioning of fluids and melts. *American Mineralogist* **84**, 1693–1710.

White, R. W. & Powell, R. (2002). Melt loss and the preservation of granulite facies mineral assemblages. *Journal of Metamorphic Geology* **20**, 621–632.

White, R. W., Powell, R. & Holland, T. J. B. (2001). Calculation of partial melting equilibria in the system Na_2O–CaO–K_2O–FeO–MgO–Al_2O_3–SiO_2–H_2O (NCKFMASH). *Journal of Metamorphic Geology* **19**, 139–153.

White, R. W., Powell, R. & Clarke, G. L. (2002). The interpretation of reaction textures in Fe-rich metapelitic granulites of the Musgrave Block, central Australia: constraints from mineral equilibria calculations in the system K_2O–FeO–MgO–Al_2O_3–SiO_2–H_2O–TiO_2–Fe_2O_3. *Journal of Metamorphic Geology* **19**, 139–153.

Willemse, J. & Viljoen, E. A. (1970). The fate of argillaceous material in the gabbroic magma of the Bushveld Complex. In: Visser, D. J. L. & von Gruenewaldt, G. (eds) *Symposium on the Bushveld and other Layered Intrusives*. *Geological Society of South Africa, Special Publication* **1**, 336–366.

Wintsch, R. P. (1975). Solid–fluid equilibria in the system $KAlSi_3O_8$–$NaAlSi_3O_8$–Al_2SiO_5–H_2O–HCl. *Journal of Petrology* **16**, 57–79.

Zheng, Y.-F. (1993). Calculation of oxygen isotope fractionation in anhydrous silicate minerals. *Geochimica et Cosmochima Acta* **57**, 1079–1091.